UNIVERSITY OF CANTERBURY

Fabrication of Dye Sensitized Solar Cells on Pre-textured Substrates

A thesis submitted in partial fulfilment of the requirements for the Degree of Master of Engineering in Electrical and Electronic Engineering in the University of Canterbury

Linda Yen-Chien Chen

2010/12/14

Supervisor: Maan Alkaisi

Contents

Figure Content

Table Content

Acknowledgements

First of all, a big thank to my supervisor Associate Professor Maan M. Alkaisi, for supervise me and give me guidance throughout my whole research, from research planning, all the way to thesis writing, giving funding for attending international conference in Japan. Other big thanks to my co-supervisor, Dr. Alan Martin for teaching me on the resistivity analysis and providing helps during the experiment when he is available. I am also very grateful for Ms. Helen Devereux and Mr. Gary Turner, for their great assistance in the nanolab, showing me how to use all the equipments that are required for my research.

The second part of the research was carried out at National Nanodevices Laboratory (NDL), Tainan, Taiwan. Special thanks to Ms. Mei-Yi Liao, for her supervision and guidance in the laboratory on DSSC assembly and characterization. Another thank to Mr. Yen-His Li, for helping me on taking SEM images in the other campus of NDL. Furthermore, a big thank to Miss Jie-Yi Yao and Mr. Mao-Nan Chang from NDL. Hsing Chu, for the assistance on Al:ZnO XRD characterization.

The process of DSSC fabrication was originally provided by Professor Yu-Lang Lee's laboratory. Special thanks to Professor Lee and his group for allowing me to use the equipments in their lab and for the fabrication recipe. Another credit to the Nano and Mems Laboratory at the department of Aeronautics and Astronauts, National Cheng Kung University, Tainan, Taiwan for allowing me to use their solar simulator system when the system provided by NDL were temporarily down.

I would also like to thank my parents for financially assisting me during my master research enabling me to return to Taiwan for the second part of my research as well as go overseas for attending international conferences. Special thanks to the New Zealand Federation of Graduate Women as they have partly funded me for my trip to overseas for the conferences.

ABSTRACT

Dye Sensitized Solar Cells (DSSC) possesses huge potential in solar energy utilisation and immense research has been carried out in order to improve its performance. There are several aspects that affect the solar cell's performance, such as the photon collection efficiency of the cell, the reflectivity of the semiconductor, the transparency and conductivity of the transparent conductive oxide layer, and the photon-electron conversion efficiency. In this research, a pre-patterned substrate was used as a base to fabricate DSSC for improving the photon collection efficiency of DSSC. The pre-patterned substrate was prepared using maskless dry etching technique, resulting in micro-size features on the substrates and giving a 1% reduction on reflectance. The effect of Aluminium doped ZnO sputtered as the Transparent Conductive Oxide layer (TCO) in comparison with a typical DSSC fabricated on Tin doped Indium Oxide glass (ITO) was also studied. The research was carried out in two parts: substrate texturing of glass fabrication with Al:ZnO deposition, and DSSC cell assembly. The first half was carried out in the nanofabrication laboratory at University of Canterbury, New Zealand, and the second half was in National Nano Device Laboratory, Taiwan. The characteristics of both the substrates and the cells were measured using spectrophotometer with integrating sphere and solar cell simulation system. Decrease in reflectance of the Al:ZnO coated substrate at infrared region from 20% to 10 % was achieved. Due to the high resistivity of Al:ZnO and the problem of incapability in TiO_2 coating, DSSC cells fabricated with these substrates have efficiencies around 2%, which is lower than the typical DSSC cells fabricated with ITO glass. Future adjustments on the substrate etching process and the cell assembly are needed for optimizing the results. The relatively high resistivity of Al:ZnO also needs to be lower for better DSSC cell performance.

1. INTRODUCTION

Energy consumption is one of the most important aspects in people's everyday life. It exists in different forms, from burning woods to obtain fire in prehistoric times to electricity productions in modern age. However, due to the rapid growth in industrialization in many countries, the original sources of energy that people used to harvest from have shown signs of deficiency. Therefore, people starts searching for new resources for energy production. At the same time, people also realized the damages that the energy production has done to the environment. Therefore, researches on 'clean energy' have increased rapidly in the past 30 years. One of the most prominent clean energy is solar energy.

Modern technologies enable solar energy to be used in two different ways: thermal conversion and photo electricity conversion. Solar thermal energy can be used on heating systems such as water cylinders or household heaters. Photo-electricity conversion, in the other hand, can be used on household or industrial electricity power generation, might one day replace the conventional thermal power generation, and can decrease the amount of fossil oil required, resulting in an extension of the date when the fossil fuel is used up.

Photo-electricity conversion converts solar light into electricity by utilizing the energy from photons to break off the bond between the atom and the electrons so that the electrons become free electrons. A solar cell, silicon crystalline solar cell for example, contains an n-type silicon and a p type silicon combined together, so that the free electrons from n type silicon can be attracted to the holes in p type silicon and create electron pairs. As the photon enters the material, it separates the electron pairs into free electrons and holes. With a little help from the electric field at the pn junction, the separated electron and hole flows in opposite directions away from each other, into the electric load without recombining with each other.

Of all the different types of solar cells, crystalline silicon solar cell is the dominant type of cells used in power generation due to its high power efficiency. However, the high cost of the silicon wafers lead the scientists to explore other types of solar cells, including thin films, CIGS, III-V, organic and dye sensitized solar cells. Apart from this, the high reflectance of silicon wafers contributes to the limits of the performance of the cells. Therefore, researches on light trapping techniques such as adding an anti reflection layer on the substrate or using dry etching and wet etching techniques to texture the substrate surface were also developed in the hope of

increasing the devices' performance.

1.1 The Aim of This Project

This thesis focuses on the possibility of fabricating maskless surface texture on glass substrate before the deposition of the Transparent Conductive Oxide (TCO). The textured substrates were then assembled into Dye Sensitized Solar Cell (DSSC) and the sample performances are compared with the DSSC fabricated in standard procedures provided by Prof. Lee's laboratory at the Department of Chemical Engineering, National Cheng Kung University in Taiwan.

1.2 Thesis Outline

Chapter 1:
History reviews of solar cells, DSSC, light trapping and TCO will be given, as well as the current status of research progress in each area.

Chapter 2:
The working mechanisms of DSSC, surface texturing, and the related Al:ZnO characteristics from the literature will be given. The mechanisms of major fabrication process used during the research, such as RIE and sputtering, will also be discussed in this section.

Chapter 3:
A detailed description on the experimental procedures carried in this research will be provided, including the equipment models used and the condition settings.

Chapter 4:
This chapter focuses on the results and observations made during the research. The obstacles of the fabrication process and methods of overcoming these problems have also been given in this chapter.

Chapter 5:
A description on the research application and possible future works are described followed by the conclusion of this thesis.

A list of references is given at the end of this work for further readings.

This research work has been included in the poster presentations in two international conferences:

1. International Conference on Nanophotonics 2010, May 28-30, Tsukuba, Japan
   (P-B88) Light Trapping Technique for Dye Sensitized Solar Cell
2. IEEE 35th Photovoltaic Specialists Conference 2010 (PVSC 35), June 19-24, Honolulu, USA
   (842-P32) Fabrication of Dye Sensitized Solar Cell with Surface Textured Substrates

The research paper was also been accepted by the Journal of Non-linear Optical Physics and Materials (JNOPM) but has not published yet.

1. (#609-2) Light Trapping Technique for Dye Sensitized Solar Cell, by Linda Y. Chen, Maan M. Alkaisi and Mei-Yi Liao

1.3 Types of Photovoltaic cells

Photovoltaic cells are devices that can transform the energy of the sun light into electricity. Theories of photovoltaics can be dated back to early 1800s. In 1880, Charles Fritts made the very first photovoltaic cell that contains selenium and a very thin layer of gold. [1] However, the power efficiency was so low at the time that not that many scientists were very interested in it. It was only until 1954, when Bell Lab announced that they have produced a silicon solar cell with over 6% efficiency, that various researches on solar cells were developed. [2] Currently, the silicon crystalline solar cells still dominate the industry due to the cell efficiency, as shown in Figure (1).

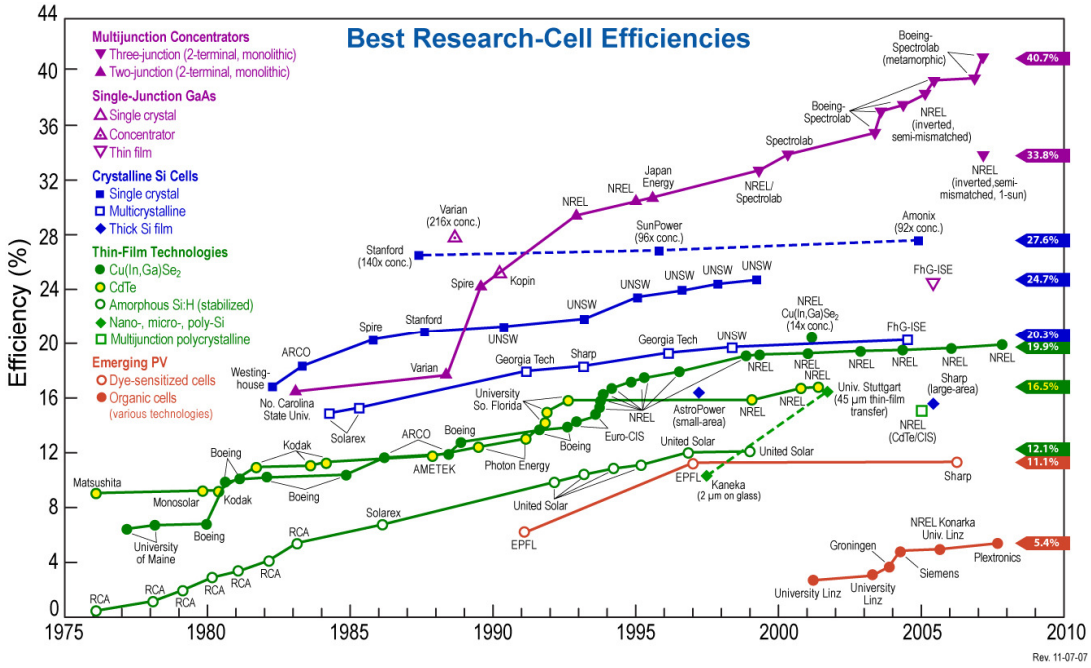

Figure 1 Chart of photovoltaic cell developments from 1975 to 2010 [3]

They could be roughly categorized into four categories: silicon based crystalline solar cells, thin film solar cells (silicon based and amorphous silicon), compound material solar cells and photochemical solar cells. A brief description of different solar cells is given below:

1.3.1 Mono-crystalline and Poly-crystalline solar cells

Silicon solar cells were invented by Russel Ohl in 1941 [4]. However, the first actual silicon solar cell module was built by Bell Lab researchers: Gerald Pearson, Calvin Fuller and Daryl Chapin [5]. The structure of the cells is simply a silicon p-n junction. Both Mono and poly-crsytalline cells require long fabrication processes

and require massive amount of silicon material. Mono crystalline solar cells, with continuous and unbroken crystal lattices, are generally grown from cylindrical ingots that are grown by Czochralski process. Poly-crystalline cells, on the other hand, are generated simply by casting the silicon ingots that are made from cooling and solidifying the molten silicon. The performance of the cells can achieve efficiency as high as 25% for monocrystalline and 18% for polycrystalline in laboratory researches, which is close to the theoretical optimal efficiency. Commercialized cells have also achieved 12% efficiencies.

1.3.2 Silicon Thin Film Solar Cell

Silicon thin film solar cells are another type of polysilicon cells. Instead of cutting slices from silicon ingots, the materials are deposited onto low cost substrates, such as glass and ceramic, using technologies like Plasma Enhanced Chemical Vapor Deposition (PECVD), with a certain thickness. There are three types of silicon thin film cell structures: single junction, twin junction and multiple junctions. The major difference between these structures is the number of p-i-n junction layers in the cell. These types of solar cells require less material and simpler fabrication than crystalline cells but still maintain the characteristics of crystalline cells such as high absorption in visible light range and good light stability, preventing light induced degradation to occur. The only downside of this type of cell is that its efficiency is still very low in comparison with crystalline solar cells. [6]

1.3.3 Amorphous Silicon Solar Cell

In 1976, Pankove and Carlson reported the first amorphous silicon solar cell with 2.4 % and the efficiency was soon improved to 4 % [7]. What makes amorphous silicon differ from crystalline silicon is the lack of long range well ordered lattice that exists in crystalline silicon. The cells can be produced on cheap substrates such as glass or plastics. The thickness of the cell is very thin, even less than $1/100^{th}$ of crystalline silicon cell thickness, reducing the cost of silicon material. Moreover, the cells can be fabricated under low temperature, reducing the energy consumption during the fabrication process and hence lower the fabrication cost. Currently, a-Si solar cells in the world are able to produce 50 MW per year and have been utilized on watches, calculators and independent power generation centre.[6] Because of the low in efficiency—approximately 10% in large scale fabrication and 13% in laboratory researches, there are researches focusing on improving the cell design, either by improving the fabrication technology and by develop new amorphous alloys.[7-10]

1.3.4 CIS and CIGS Solar Cell

Researches on Chalcoprite based solar cells began in early 1970s and the research group lead by Dr Goryunova was the pioneer of this area. The cells can be separated into two main categories: $CuInSe_2$, short for CIS, and Cu $(In_{1-X}Ga_X)$ $(Se_{1-Y}S_Y)_2$, short for CIGS. Although the efficiency of the cells are lower than the siicon crystalline (20% in comparison with 25%), its advantages such as low material costs, wide light absorption range and good stability draw the public attentions, resulting in massive research.[11] For these types of cells, the ratio between Ga/(Ga+In) and Se/(Se+S) for CIGS and the ratio between Se(Cu+Se) and In/(Se+In) for CIS are important aspects in controlling the band gap width and the phase type that are directly related to the conversion efficiencies. The cell structures are in sandwich form, shown in Figure (2). There are several ways in fabricating the CIS or CIGS compound layer, such as Metallic Organic Chemical Vapour Deposition (MOCVD), Vacuum Evaporation, Chemical Bath Deposition (CBD) and more.[12]

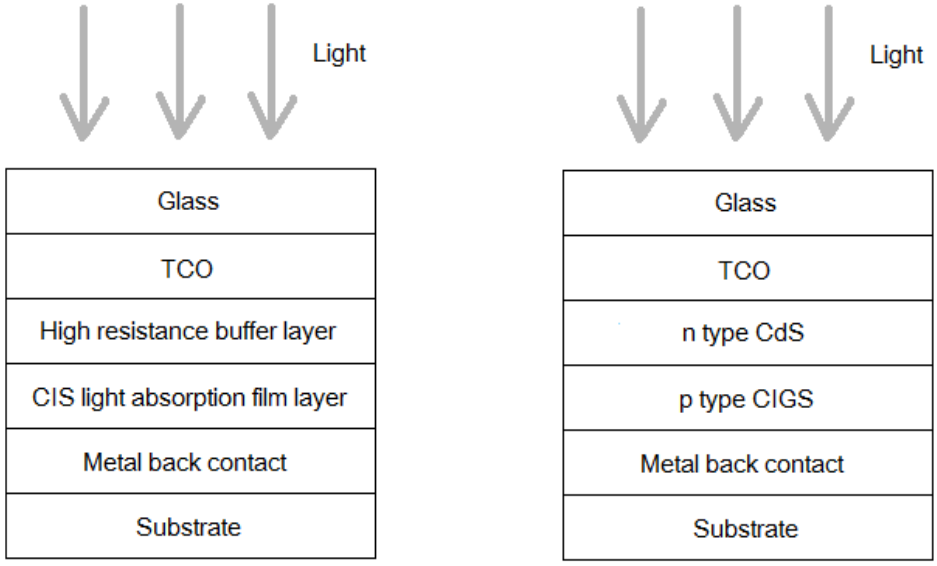

Figure 2 Left: CIS solar cell structure; Right: CIGS solar cell structure

1.3.5 CdTe Solar Cell

CdTe based thin film solar cells are formed by connecting p type CdTe and n type CdS together. Both materials are direct band gap semiconductors, good for generating electron–hole pairs and reducing the percentage of electron-hole pair recombination. Due to the fact that the theoretical efficiency of the cell is around 29% and the structure of the cell is simple, the device was quite popular in research groups. It is a device with high efficiency and low fabrication cost. The structure

of the cell is shown in Figure (3).

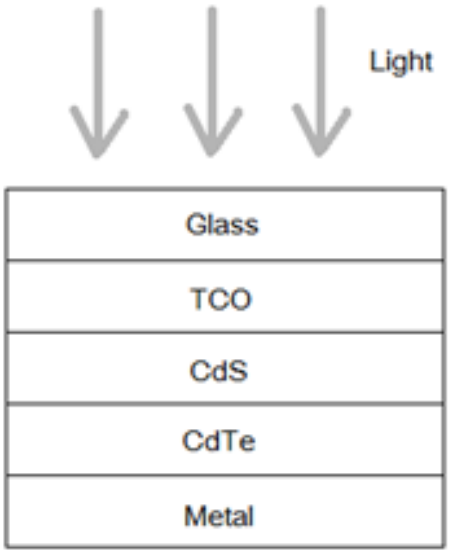

Figure 3 CdTe Solar cell structure

There are seven methods in fabricating CdTe thin film: Electro-Deposition (ED), Closed-Space Sublimation (CSS), Screen Printing (SP), Spray Deposition (SD), Vapour Transport Deposition (VTD), MOCVD and Sputtering.[13-16] However, method such as CSS, because of its capability in determining precise amount needed in forming CdTe, requires higher fabrication cost and thus is normally not used in large production. SD, on the other hand, is simple and does not need to be done in vacuum environment, so companies like Golden Photo have managed to industrialize this method. The efficiency of the cell produced by Golden Photo has reached around 8%.

1.3.6 Photoelectrochemical Solar Cell

Photoelectrochemical cells, including dye sensitized solar cell and organic solar cells, utilize photochemical reaction to generate electricity. This type of cell has a number of advantages such as low mass production cost, good alterability in material structure, and wide range in visible light absorption. Some materials used for this type of cells are said to be reproducible. Furthermore, the cells are much less sensitive to the semiconductor defects than the conventional crystalline cells. The structure of the cell is normally in sandwich structure, with transparent substrates as the top and bottom layer and transparent conductive oxide (TCO) layers as conductor. This type of solar cell will be investigated in this thesis work. [12, 17, 18]

1.3.7 Third Generation Solar Cell

According to Prof. Green [19] from the School of Photovoltaic and Renewable Energy Engineering at University of New South Wales, Australia, the term 'Third Generation Solar Cell' refers to solar cells that are fabricated with the most advanced technologies and PV devices that operate differently in theory to conventional semiconductor PV. New technologies and theories such as quantum dots , hot carriers [20, 21], tandem cells [22-24], thermal photonics [25], and more have been discovered in the past few years, aiming at finding an alternative way of utilizing solar power in a more cost effective way compared with the crystalline and thin film cells. The concepts for third generation solar cells are based on overcoming the theoretical solar conversion efficiency limit for a single junction material, calculated by Shockley and Queisser in 1961. Currently, these types of photovoltaic cells are still in theoretical laboratory research level. Commercialization is still quite a long way to go. Figure (4) shows the theoretical efficiency expected for each type of third generation PVs proposed by Prof. Green. [19]

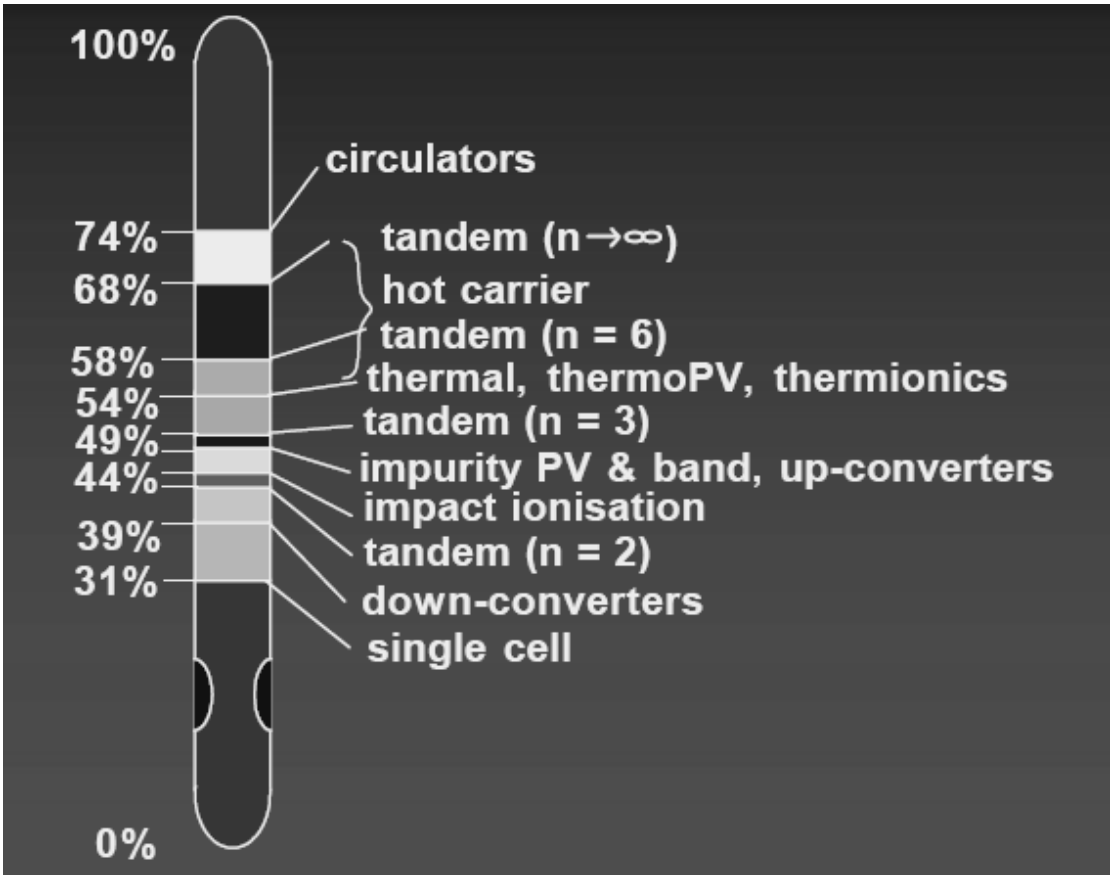

Figure 4 Third genration solar cell efficiencies [19]

1.4 Dye Sensitized Solar Cell (DSSC)

DSSC is a type of photoelectrochemical cell, as described in section 1.3.6. Wide band gap semiconductors are used as electrode for the cells due to their high photochemical stability. However, this type of semiconductor does not have the ability to absorb visible light. Therefore, photo sensitizers such as dye particles are added to the material to absorb visible light.

1.4.1 History

The history of DSSC begins with two different aspects that were later converged into one: photography and photochemistry. The first panchromatic film was produced based on the research, about the association of dye and halide semiconductor, lead by Vogel in Berlin in 1870s. Soon after that the first photo-electrode was developed with similar photochemical theory. In 1887, James Moser reports dye sensitized photochemical cell, the prototype of DSSC nowadays [26]. In 1960s, the research of dye for photochemical cells has come to an important milestone: the verification that the cell operates by injecting electrons that are excited by photons into the conduction band of the n-type semiconductor. Moreover, in 1964, during the International Conference on Photosensitization on Solids in Chicago, an amazing realization that the same dye can be used in both photography and photo-electrochemistry fascinated many chemists. The efficiency of the cells was limited under 3 % for a very long time due to the fact that maximum efficiency of the cell can only be obtained if dye material was closely packed with TiO_2 particles in monolayer. It was only until 1991 when Grätzel and O'Regon announced the development of DSSC with 7% efficiency, using nanometer size TiO_2 [18]. Approximately 10 years later, with the development of better dye materials, the performance of DSSC improved to over 10% efficiency [27].

1.4.2 DSSC Current Research Progress

A typical DSSC cell structure and its operational principles are shown in Figure (5) below. The oxide semiconductor material, typically TiO_2, is used for light absorption and electron transfer. However, due to the fact that the material is a wide band gap semiconductor, much shorter wavelength (UV range) is required for electron excitation. Therefore, light sensitive dye material is used to coat the semiconductor material for electron excitations within visible wavelength range. The liquid electrolyte is used to regenerate electrons for dye material for long stability purpose.

The cathode layer, usually a thin Pt coating, is used to transfer the electrons from the load to the liquid electrolyte for oxidation-reduction process (REDOX).

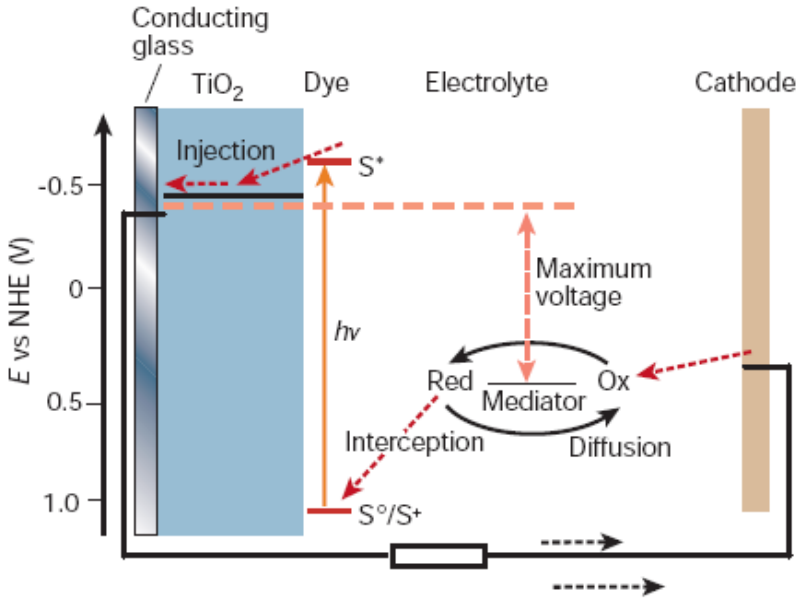

Figure 5 Basic structure of DSSC and the function of the materials [26]

Researches on DSSC can be classified into various fields: Semiconductor structure and material, Liquid or solid electrolyte material, Dye material, TCO and industrialization aspects. A few directions are introduced below:

Semiconductor Structure and Material

The most commonly used wide band gap semiconductor in DSSC is TiO_2. However, studies show that this material may have achieved its optimum performance. Therefore researches on different semiconductor material as the electrode have been investigated. ZnO is the most commonly used material as the substitution for TiO_2. Furthermore, investigations on the material's structure have been carried. This includes fabricating TiO_2 in nanotube or nanowire structure. Moreover, researches on whether TiO_2 is in colloidal form or sol-gel form were also very popular. Colloidal form TiO_2 is easier to prepare as it can be prepared from already made TiO_2 powder and requires less chemicals than sol-gel method. Preparation with sol-gel method can produce particles with smaller diameters, and good chemical uniformity. However, the main downside for this method is the toxic solvents. [28-31]

Electrolyte Material

Liquid Iodide/triiodide is the most commonly used electrolyte material for DSSC. However, liquid electrolyte often causes leakage problems and degrades very fast

photochemically resulting in short lifetime for the cell. Solid state electrolyte was then been investigated but was soon discovered that it may suffer from poor transparency, which is one of the most important conditions required for DSSC. Therefore, development of quasi-solid state electrolyte such as gel type has been carried out, aiming at providing DSSC cells with better stability. Prof. Segawa's team from University of Tokyo announced that the smectite clay technology may be able to solve the long term problems.[32]

Dye Materials

One of the biggest problems in DSSC fabrication is its material cost, causing high price for electricity generation. This is mainly due to the cost for dye material (range from $AUD 1000 to $AUD 3000 per gram).[33] The dye materials commonly used in laboratory are expensive patented Ru dye or N719 dye, developed by Grätzel's research group. Although these dye materials have wide photon absorption range, they could only be used in DSSC cell fabrications as it is prepared especially for DSSC. In consequence, it is very difficult to lower the fabrication cost. Therefore, alternative dye materials such as organic dye chemicals are developed. Organic dye ($NT 50 per gram) is much cheaper and more environmental friendly than inorganic dye.[34] Moreover, as new fabrication technologies being developed, various researchers turn their focus back to semiconductors and therefore research projects such as using semiconductor quantum dots as sensitizers for DSSC has developed.[35, 36]

1.5 Light Trapping Technique

One of the biggest energy lost in solar generated electricity is the amount of light being reflected before entering the cells. Therefore, light trapping technique became an essential tool in PV cell design. The use of light trapping technique was first appeared in astronomical instrument history in late 1800, long before the fabrication of the first solar cell. Dennis Taylor[1] discovered that old lens managed to transmit more light than newly polished lens due to a thin tarnish layer, oxidized through time, on the old lens. The phenomenon was explained through optical theory such that the tarnish layer consists of lower refractive index than the lens itself, resulting in the reduction of optical loss.[37] A patent of using various acids to wet etch the lens, in order to fabricate the tarnish layer deliberately was filed in 1904. Since then, various researches on light trapping technique were carried out. However, during that time,

[1] Dennis Taylor (1862-1943) was a famous optical designer who worked for the T. Cooke & Sons. He was granted with approximately 50 patents for optical and other instruments.

the focus of the researches was on anti-reflection layer.[38] Surface texturing began only about half of the century later that Calvin Fuller[2] filed a patent with a description of improving the performance of solar cell with rough top surface. The topic reached its milestone in 1960 when Dale and Rudendberg[3] drew the photovoltaic community's attention onto the possibility of using patterned surface structure to minimize the reflectance of the devices.[39] Different patterns of surface texturing were tried out and such technique has become one of the essential parts of fabricating a photovoltaic device with good characteristics.

1.5.1 Thin Film Anti-reflection

Anti-reflection technology was a top secret in German military after Dennis Taylor's discovery until in 1938 when Katharine Blodgget[4], a researcher at General Electronics discovered that a 99% transmittance glass can be obtained by depositing organic films with thickness controlled, layer by layer, on the glass substrate. The coatings are categorized in two categories: single layer and multi layer. The mechanisms are similar, as shown in Figure (6), but multi layer coatings can cover larger range of wavelengths whereas single layer coatings could only interferes certain light wavelength regions.

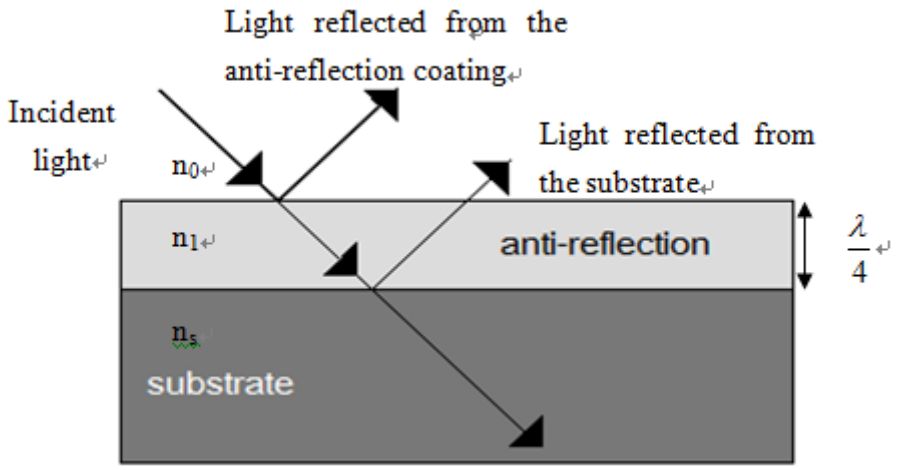

Figure 6 The Operation theory of anti-reflection coating showing incident light being reflected from the anti reflection coating and the substrate.

The transmittance of the coated substrate, T, varies only within the range of 0 (no

[2] C. S. Fuller, "Fabrication of Semiconductor Devices," in *Us patent* 2,794,846, 1954.
[3] H. G. Rudendberg and B. Dale, "Radiant Energy Transducer" in *US patent* 3,150,999, 1961.
[4] Katharine Blodgget: One of Ernest Rutherford's student who worked at General Electronics filed the patent US patent #2,220,660 for "Film Structure and Method of Preparation" for anti reflection coating.

light transmitted) and 1 (all light transmitted). If light absorption and scattering are neglected, then the transmittance is always 1-*R*, where R is the reflectance of the coated substrate. The theoretical optimum transmittance, T_{max}, can therefore be derived from the following equations [40]:

$$T_{max} = \frac{4n^2 n_0 n_1}{\left(n_0 n_1 + n^2\right)^2} = 1 - R_{min}, \text{ when } \phi = 90°, 270° \text{ etc.} \quad (1)$$

R_{min} it the minimum reflectance of the coated substrate, n_0 is the refractive index of air and n_1 is the refractive index of the substrate. Therefore, to obtain zero reflectance, $R_{min} = 0$, the refractive index value of the thin film antireflection coating need to have the following relationship with the air and the substrate.

$$n = \sqrt{n_0 n_1} \quad (2)$$

Moreover, under this condition, the thickness of the film should be the multiples of 1/4 incidence wavelength such that

$$nd = \frac{\lambda}{4}, \frac{3\lambda}{4} .... \quad (3)$$

1.5.2 Substrate Surface Texturing

After Calvin Fuller's discovery of efficiency improvement with rough top surface, several methods of fabricating textured surface were published in the past decades. Dobrzański *et al.* [41] categorized the methods into three categories: acid texturisation, reactive ion etching and mechanical texturisation. Acid texturing, using chemicals such as HF and KOH, can be done in short time, as fast as few seconds, but the major drawback is that precise pattern and large scale reproduction are difficult to acquire. Moreover, large amount of chemical waste produced during fabrication. Dry etching, on the other hand, provides patterns with better precision but requires longer time to process. Mechanical texturing is effective only on certain materials. Various types of surface pattern have been published, including pyramids, and hexagonal holes. Researches on surface texturing are abundant especially for silicon thin film solar cells. Most of them are fabricated directly on silicon, or on TCO. Direct surface texturing on glass substrates for other thin films are difficult to find. The operation principles of surface textured light trapping have been discussed in various literatures. Martin Green[5] specifically described this technique into one chapter in his book

[5] Martin Green: A pioneer in photovoltaic researches. His publications have been widely cited by researchers in photovoltaic aspects.

published 15 years ago [42]. A more detailed operation mechanism will be discussed in chapter 2.

1.6 Transparent Conductive Oxide (TCO)

Due to the special characteristics of high transparency and low sheet resistance, TCO is an important material not just for solar cells but also for various applications especially in the optoelectronic field, such as flat panel displays, LEDs, and waveguide devices. TCO is a wide bandgap n type semiconductor that consists of high concentration of free electrons. The most common ones are Tin doped Indium Oxide (ITO), Fluorine doped Tin Oxide (FTO) and Aluminium doped Zinc Oxide (AZO or Al:ZnO) due to the good electrical conductivity, high transparency and the low material costs.

The research in TCO began popular about one century ago when K. Badeger published a report in 1907 proposed the method of cadmium sputtering with thermal oxidation to produce CdO thin film [43]. Since then, numerous reports on transparent film deposition emerged. Undoped SnO_2, In_2O_3 and ZnO were materials that are researched widely at the start. Doping with other materials showing much better characteristics was discovered later. Moreover, electronic devices utilizing this technique such as resistors, light trapping anti-reflection coatings, and thin film solar cells have been developed. Sixty years later, Holland reviewed the efforts that have been done in this field in his publication [44], describing the methods of fabrication , characteristics and applications

The research in TCO has not yet reaches its acme as abundant research projects are set to investigate a better TCO material with higher electron mobility. Apart from the material itself, methods of depositing TCO were also examined closely. The common processes for fabricating TCO are evaporation [45-47], sputtering [48], reactive ion etching [49], chemical vapor deposition (aka. CVD) [50, 51], spray pyrolysis [52], solution dipping , and chemical solution growth. For evaporation process, several materials are fabricated with oxidizing metal film after evaporation, with vacuum evaporation of metal material in oxygen atmosphere, or with direct thermal or electron beam evaporation. The most commonly used TCO materials are described below:

1.6.1 Tin doped Indium Oxide (ITO)

ITO is one of the most used TCO materials in industries and laboratories for the past decades due to its high transmittance (around 80% to 90%) and high conductivity. [53] However, when the material is placed at temperature over 300 °C, its conductivity drops dramatically. This is due to the decrease in oxygen vacancies in high temperature, resulting in the decrease of electric carriers. Moreover, the scarcity of the expensive Indium material resulting in high material costs. [54] In addition to that, the toxicity of the material and the ease of reacting with hydrogen plasma, cause the researchers to look for a better substitution.

1.6.2 Fluorine doped Tin Oxide (FTO)

FTO is another type of TCO that have been widely used, especially in solar cells. This is due to its good stability at high temperature and its competitive cost in comparison with ITO. SnO_2 itself is a semiconductor with very low conductivity and wide band gap (around 4 eV). An extrinsic dopant, such as Sb or F, is added into the material. Fluorine doped SnO_2 is more commonly used than the material doped with Sb. This is due to the variation in resistivity with the amount of Sb doped. Another advantage of FTO is that it has high transmittance (> 80 % or 85 % depending on the thickness), especially in visible wave region. [55] Its resistivity can be as low as 2×10^{-4} Ω-cm, depending on the thickness of the film. [56]

1.6.3 Aluminium doped Zinc Oxide (AZO or Al:ZnO)

An alternative material that has been widely discussed for ITO substitution is Al doped ZnO. ZnO is a wide band gap n type semiconductor with wurtzite structure, categorized in II-VI group. It has high exciton binding energy, approximately 60 meV, which is higher than the 25 meV of GaN. Therefore, ZnO has been a promising material in optoelectronic fields. However, undoped ZnO suffers from low conductivity (around 1-100 Ω-cm) [57], not compatible for use as electrodes. Therefore, like FTO, an extrinsic doping is normally added into the material to increase the carrier concentration, resulting in conductivity increase, at the same time, maintain the transmittance. Both Zinc and Aluminium are inexpensive and abundant material. This gives AZO an advantage when comparing with ITO as it is relatively cheap. [58] Further description on AZO characteristics will be given in section 2.1.9.

2. BACKGROUND

2.1 Principles

2.1.1 DSSC Basic Structure

A typical DSSC cell consists of two TCO coated transparent substrates, normally glass with ITO or FTO, with a nanoporous TiO_2 layer covered with dye solution in the middle of the cell. Below it are the liquid electrolyte and the counter electrode that is usually fabricated with Pt. The structure diagram is shown in Figure (7) below:

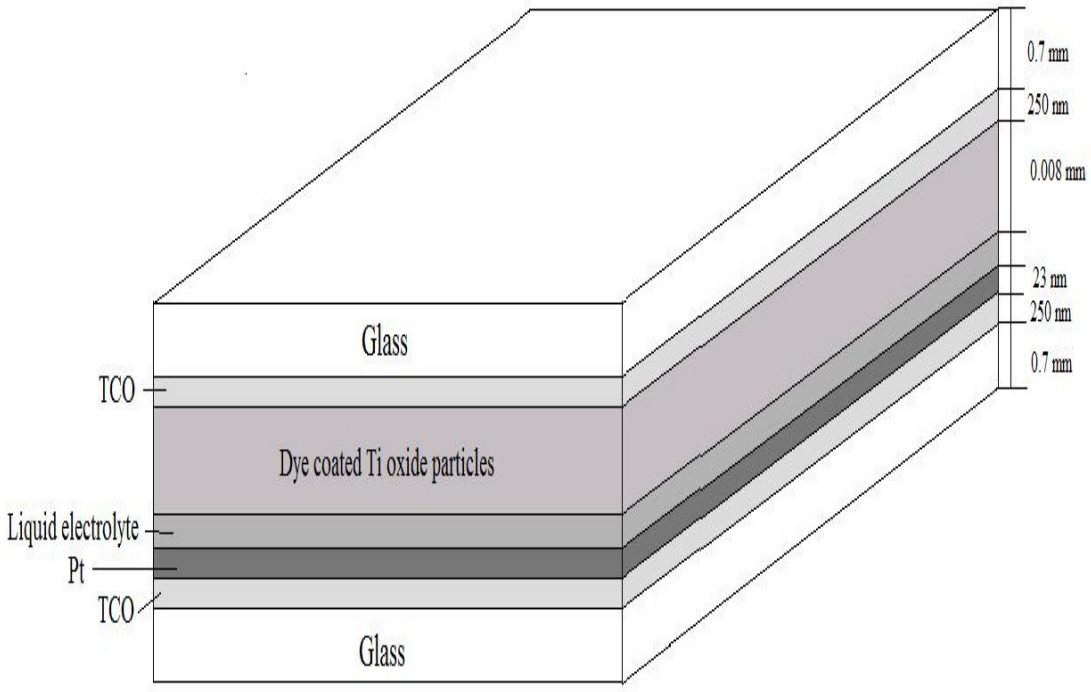

Figure 7 Basic DSSC structure with material deposition thickness. The dimension for the cell used in this research is 2cm by 2 cm

2.1.2 Operation Principle

The mechanics of DSSC is quite different to the conventional silicon solar cell. The idea was initially inspired from the photosynthesis of the leaves. The DSSC divides the whole process into two steps: light absorption and charged carrier transportation. The incident light goes through the transparent substrate and gets absorbed by the dye material, as shown in Figure (8).

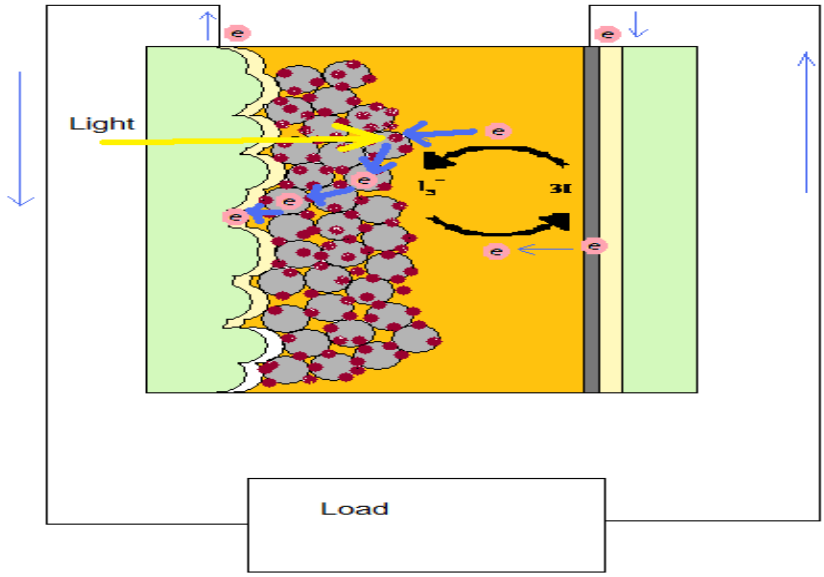

Figure 8 DSSC operation diagram: the electrons that have been excited by the photons enter the TCO layer through the conduction band of TiO_2 particles, then into the load followed by the arrows. The electrons from the load then enters the cells through the counter electrode, providing electrons for liquid electrolyte's REDOX process so that the electrolyte can return to its original state in order to donate electrons to the dye particles.

The energy of the photon excites the electron from dye particle to the TiO_2 conduction band that has lower excitation energy than dye particle. The electrons are then flow from the semiconductor, usually TiO_2, through TCO into the load. Once the electron is excited, the liquid electrolyte, usually Iodide, will oxidized into oxidation state and transfer another electron into the dye electron vacancy to regenerate the dye particle and reduce the possibility of electron recapturing by the oxidised sensitizer. Thus improves the possibility of carriers transfer to the load. The liquid electrolyte is reduced back to its original form when it accepts electron from the high conductive counter electrode, usually Platinum (Pt). Finally, the counter electrode regenerates

by accepting the electrons from the electric load. Thus, the whole operation process becomes a cycle with zero net chemical change theoretically. In overall, each inter-media contact is the most important aspect in improving the efficiency and minimising the energy loss during carrier transfer.

2.1.3 TiO_2

The main purposes of the main electrode layer are to attach as many dye particles as possible for photo-electron conversion and to transfer the generated electrons through its conduction band to TCO then to the load. The most common material used for DSSC is TiO_2. TiO_2 is a wide 3.2 eV band gap semiconductor that can be found in nature as Anatase and Rutile crystalline structures, or seldom, Brookite. Anatase is the most common structure used in high performance solar cells. Its light absorption is effective around UV waves but rather weak at visible light range. Therefore, additional photosensitive materials like dye solution is required to increase the cell's photon-electron conversion. The effective interactive surface area of the cell depends on the size of the TiO_2 particles because only the sensitizer that has direct contact with TiO_2 surface is photoactive. Therefore, by reducing the particle size, more dye particles can be attached and consequently improves the efficiency.

There are several ways in preparing TiO_2 for DSSC fabrication. TiO_2 is generally prepared in sol-gel form or colloidal form. There are commercialised TiO_2 sol-gel products that can provide high performance efficiency (over 6%) available from the industry for screen printing deposition method. However, because the material is already prepared by the manufacturer, changes of the controllable conditions of the material that are to be made are very limited. Colloidal form, in the other hand, is difficult for achieving high efficiency but there are more variables that can be controlled in fabrication. Currently, the most common way of preparing TiO_2 is by dissolving commercially manufactured TiO_2 P25 powder in deionised water. This powder contains 80% of Anatase and 20% Rutile crystalline structures. A mix of Anatase and Rutile can provide much better efficiency because Anatase crystalline has smaller resistivity and Rutile can provide photon scattering, increasing the percentage of electron excitation. The prepared colloidal TiO_2 can be deposited onto the substrate by spin coating.

2.1.4 Dye material

Small band gap energy materials are also used as dye for DSSC. This is because the photons' energy cannot be absorbed if it is smaller than the material's band gap energy. Moreover, the sensitizer needs to be stable for over 10^8 times redox reactions for long lifetime cell. The most common used inorganic materials utilized in laboratory are 3 Ru based sensitizers: N3, N719 and black dye, as shown in Figure (9).

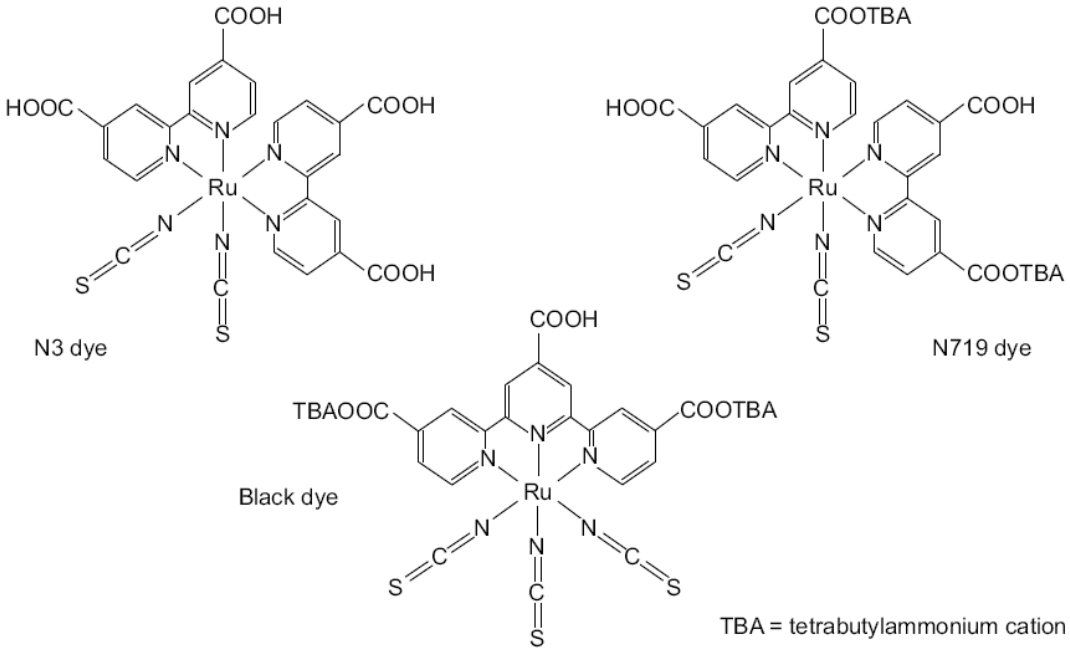

Figure 9 Chemical structure of dye materials: N3, N719 and Black dye [59]

Ru based sensitizer has a faster electron injection speed than the electron recaptured by the oxidised sensitizer. N3 dye cis-$RuL_2(SCN)_2$ (L=2,2-bipyridyl-4,4'dicarboxylate), has an optical cross section at 530 nm, giving the material the best light harvesting efficiency (LHE) compared with other sensitizers at around 99.8%. LHE is calculated using by the absorption length, α, of the sensitizer and the nanocrystalline film thickness, *d*, as shown in equation (4):

$$\mathrm{LHE}(\lambda) = 1 - 10^{-\alpha d} \tag{4}$$

The absorption length, α, can be obtained using the sensitizer's concentration in the nanocrystalline film at full monolayer coverage, σ, and the optical absorption cross-section of the sensitizer, *C*.

$$\alpha = \sigma C \tag{5}$$

However, N3 sensitizer could not absorb energies from near red spectrum. Therefore, new sensitizers such as K19 and K77 have been developed in the 4 years [60]. N719 exhibits similar characteristics to N3, but provides higher voltage for DSSC. The best dye reported so far, however, is the black dye, also developed by Grätzel's group [59].

2.1.5 Electrolyte

A comprehensive review on this subject is given by [61]. Electrolyte is the material that filled between the spaces of the nanoporous electrode. The purpose of electrolyte is to donate electrons to oxidised sensitizer to prevent the excited electrons recaptured by the sensitizer. It has to be a transparent material that allows the light to go through and, at the same time, has good conductivity and fast redox reaction. Moreover, it needs to have long term stability in many aspects including chemical, optical and especially the interfacial stability that relates to desorption and degradation of dye from oxide film. The most commonly used is liquid iodide/triiodide redox couple dissolved in organic solvents. Organic solvent is the major material that gives the iodide/triiodide ion dissolution and diffusion environment. [61]

2.1.6 Counter Electrode

Counter electrode in DSSC needs to provide high conductivity as it needs to provide the liquid electrolyte electrons to complete the redox reaction in very short time for lifetime stability and preventing the electron recapture. Currently, the most common used material is Pt. This is because Pt has high electron mobility that can regenerate the electrolyte rapidly. Moreover, literatures show that, for example, using gold as the counter electrode and found that the electrolyte corrodes gold [35]. Pt, on the other hand, has high stability against electrolyte's corrosives characteristic.

2.1.7 DSSC Assembly

Apart from the materials used in fabricating cells and the methods of processing them

onto the substrates affects the solar cell overall performance, the technique of how to assemble the TiO_2 deposited substrate and the Pt coated substrate together is another essential aspect in DSSC fabrication. A space or gap need to be present between the TiO_2 electrode and the counter electrode for electrolyte injection. The size of the gap determines the amount of liquid electrode being injected. This space is provided by the spacers placed around the active working area. Therefore, the material has to be thicker than dye absorbed TiO_2 electrode thickness. Moreover, as it was mentioned in the section Counter Electrode that the electrolyte has corrosive characteristics, the stability of the spacer material from the corrosion is essential. In addition to that, the method of injecting the electrolyte into the space also determines the cell's performance since improper injection may cause air bubbles stuck inside the cell. Therefore, two narrow channels from the edge of the substrate to the two opposite sides of the active working area are normally used in research for easy electrolyte injection and air bubble removal. [35]

2.1.8 Surface Texturing

TiO_2 particles in DSSC also serve a light trapping purpose, trapping the incident light that went pass the TCO coated transparent substrate inside the cells. Surface texturing for light trapping purpose normally based on randomizing scheme or geometrical scheme [42]. However, this is calculated based on silicon crystalline material, with light being absorbed into silicon. For DSSC, surface texturing is fabricated on plain glass before applying TCO layer, resulting in a different theoretical calculation. The closest simulation of light scattering from textured surfaces was given by M. Green, showing the internal paths of light when the glass substrate with rough surface is attached to a semiconductor [42].

2.1.9 Al:ZnO

ZnO is a II-VI wide band gap semiconductor with 3.37 eV band gap energy. It has high transmittance at visible light range and has wurtzite structure with great isotropic characteristics, as shown in Figure (10). However, ZnO's conductivity is limited, due to the low concentration of carrier. Doping Al^{3+} can increase the carrier concentration by taking over Zn^{2+}'s place or fill up the structure's vacancies, reducing the material resistivity. For every Zn^{2+} that has been replaced by Al^{3+}, there is one free carrier available for TCO. Therefore, AZO has much better conductivity than

undoped ZnO. However, Al^{3+} also serves as ionized impurity scattering centre in the structure, so there is a possibility that the structure changed due to the Al^{3+} vacancy filling. Therefore, it is important to control the percentage of Al doping in ZnO. The most common used in literature is 2wt% of Al [62].

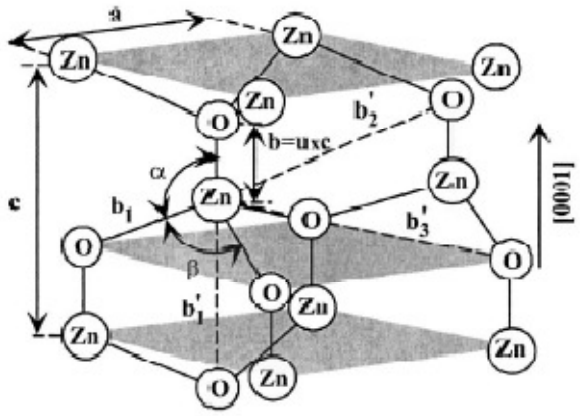

Figure 10 ZnO wurtzite structure [63]

2.2 Nanofabrication Technology

For the fabrication of textured substrates used for the assembly of the DSSC, a number of process and techniques are required. In this section, a description of the main equipments that have been used in this study will be presented.

2.2.1 Reactive ion etching (RIE)

Reactive ion etching is a combination of physical and chemical etchings. Physical etching occurs when the positively charged ions and negatively charged electrons are accelerated towards the sample due to the potential difference created by the electrode. The chemical etching uses the plasma to produce charged particles that reacts with the materials on the sample. The reaction between the charged particles and the material produces gas that can be extracted from the process. The advantage of RIE is that the vertical etching speed is much faster than the horizontal etching speed, minimising the undercut of the pattern. Moreover, such fabrication technology also exhibits high selectivity. Therefore, this method is normally used to form surface textures for silicon solar cell light trappings.

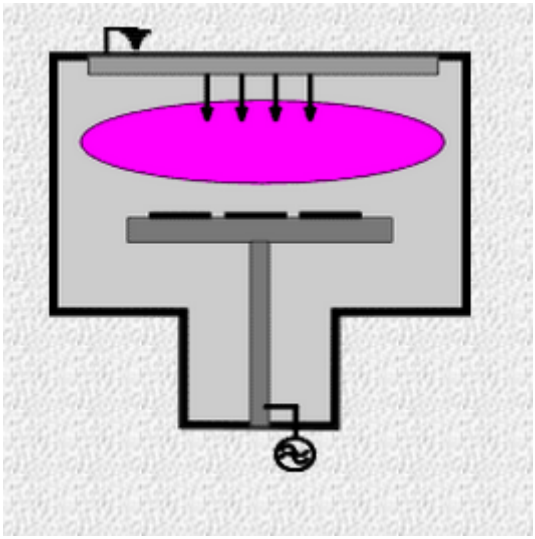

Figure 11 Basic RIE structure--samples are placed on the RF driven substrate electrode that has water cooling system connected. The top electrode has shower head gas inlet for the required gas. [64]

The schematic of Figure (11) shows the features for RIE system used in this research. Two parallel plates are the top electrode with shower head gas inlet and lower electrode for holding the samples. The space in between is where the plasma occurs. The removal of atoms of the material on the sample is done by physical collision and chemical reaction between the ions and the material on the sample to form volatile gas. An electric discharge process occurs with plasma generation during the etching process. The plasma is formed with reactive particles and neutral particles, such as ionised atoms or molecules and electrons. A low charge density region created by the electron recombination is adjacent to the chamber surface. Positive ions are accelerated due to the fields developed by the low charge density region from the plasma to the sample and bombard with the sample material. Moreover, the charged particles chemically react with the material, producing volatile gas that can be removed from the chamber by the pump. [65]

2.2.2 RF magnetron sputtering

A RF magnetron sputtering system is a type of physical vapour deposition that operates in a similar way to RIE but the target and the sample are placed in opposite way. This method is best used for depositing thin oxide materials when the process is powered by RF source. It uses the charged ions or electrons to bombard the target surface so that the particles are sputtered from the target then condensed onto the

sample. There are magnets at the cathode plate, introducing the magnetic field into the sputtering chamber, as shown in Figure (12). Argon atoms collide with electrons swinging in the magnetic field and electrons that are originally bound to the atom are knocked out from the atom, resulting in charged argon ions. The charged ions are bounced toward the target surface in high speed causing the particles at the target surface to detach. The target particles are then condensed onto the sample forming the desired film thickness.[66] The Al:ZnO layer of DSSC for this research was deposited using RF magnetron sputtering.

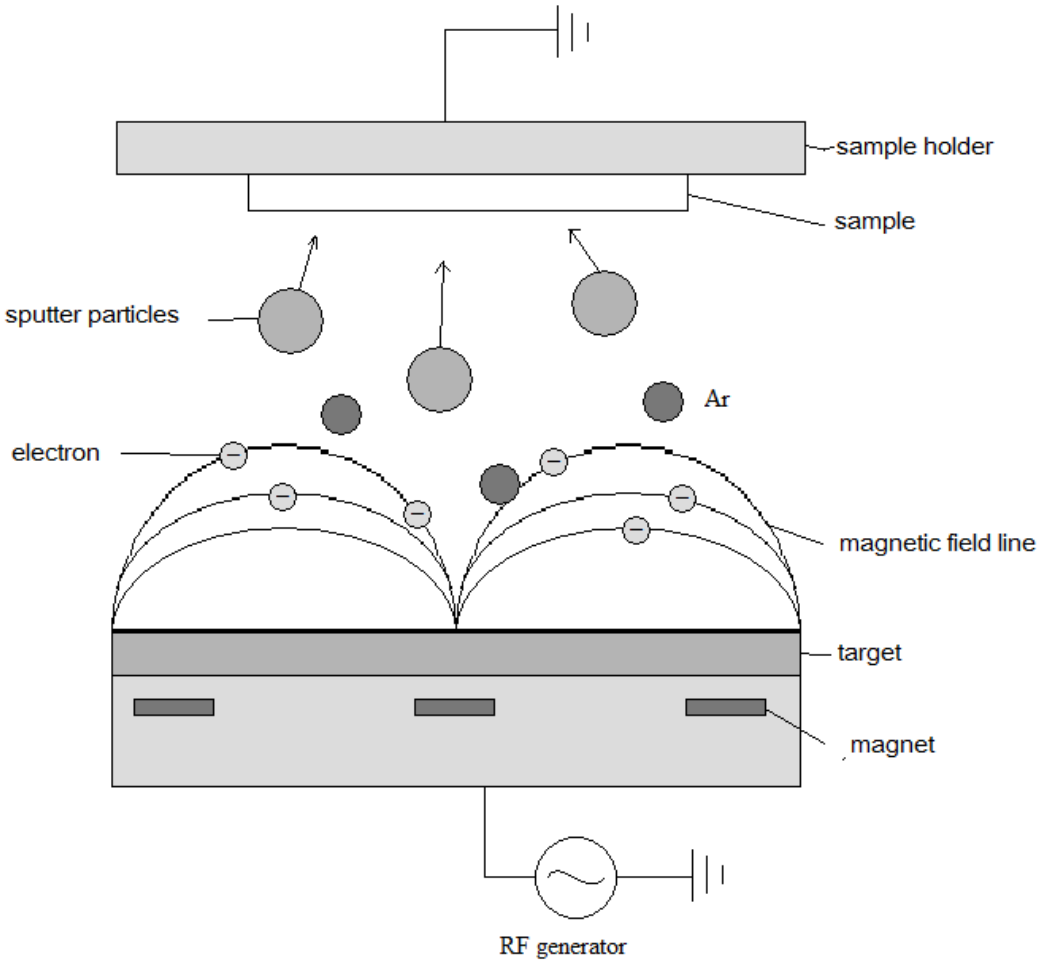

Figure 12 RF magnetron sputtering operation mechanism

2.2.3 DC Magnetron Sputtering

The suitability of magnetron sputtering varies depending on the target material. Metal materials are usually deposited using DC powered magnetron sputtering and semiconductors and oxide materials are done by RF powered sputtering. If DC power is used in depositing semiconductors, charges builds up in the target and lead to forming a shield in electrical field, consequently, causing the ion current to diminish and fade away. Therefore, DC source is only used on depositing metal materials such as Aluminium, Silver, and Gold. For semiconductor material such as silicon, silicon oxide and zinc oxide, RF power provides an AC voltage to the target, preventing charge to build up on the target. [66, 67]

2.2.4 Spin Coating

Spin coating is commonly used in micro and nanofabrication when depositing liquid materials. The sample is placed in the middle of the spinning disk with vacuum pump to keep the sample in place, as shown in Figure (13).

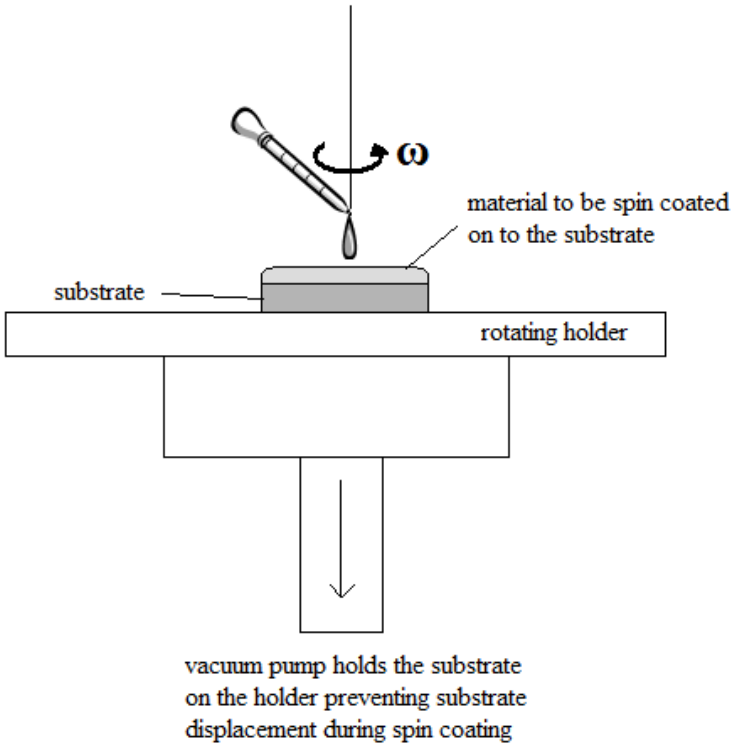

Figure 13 Spin coating process for uniform material deposition

The deposited film thickness is mainly controlled by the spinning speed of the equipment and the viscosity of the material. The higher the spinning speed and the lower the viscosity would give thinner film thickness. The excess material is either got spin off from the sample or is build up on the edge of the sample. The length of spinning affects the film's distribution on the sample such that the longer the spinning time, the more the spin off excess material and the less material build up on the edge. However, this is also affected by the speed of material solidifying and solvent evaporation. When the material solidifies too fast, it may require higher speed or acceleration of spinning to obtain the required thickness. [68]

2.3 Material Characterization Technology

2.3.1 Atomic Force Microscopy (AFM)

The technology was invented by the Nobel Laureates: Binnig, Quate, and Gerber in 1982 [69]. It is a type of scanning probe microscopy technology. It can scan the material in *x, y,* and *z* dimensions, if required, giving a 3D image of the substrate surface topology. The resolution of the microscopy ranges from 01 to 1 nm for *x*, *y* planes and 0.01 nm for the *z* plane. The technology could also work in liquid environment, therefore is useful for material analysis and especially, biology or micro-fluidic applications. There are several different modes of sample measuring using AFM. The one that was used in this research is the contact mode, which is the most widely used in AFM characterization. The microscope measures the surface by measuring the force between the surface and the probe. The probe is connected to a cantilever that is pressed against the sample with a very tiny force (inter-atomic force range). By controlling the piezoelectric actuator, the tip can move back and forth across the sample. A laser beam aiming at the back of the cantilever is reflected from the cantilever to a photodiode detector that records the cantilever's deflection, as shown in Figure (14). [69]

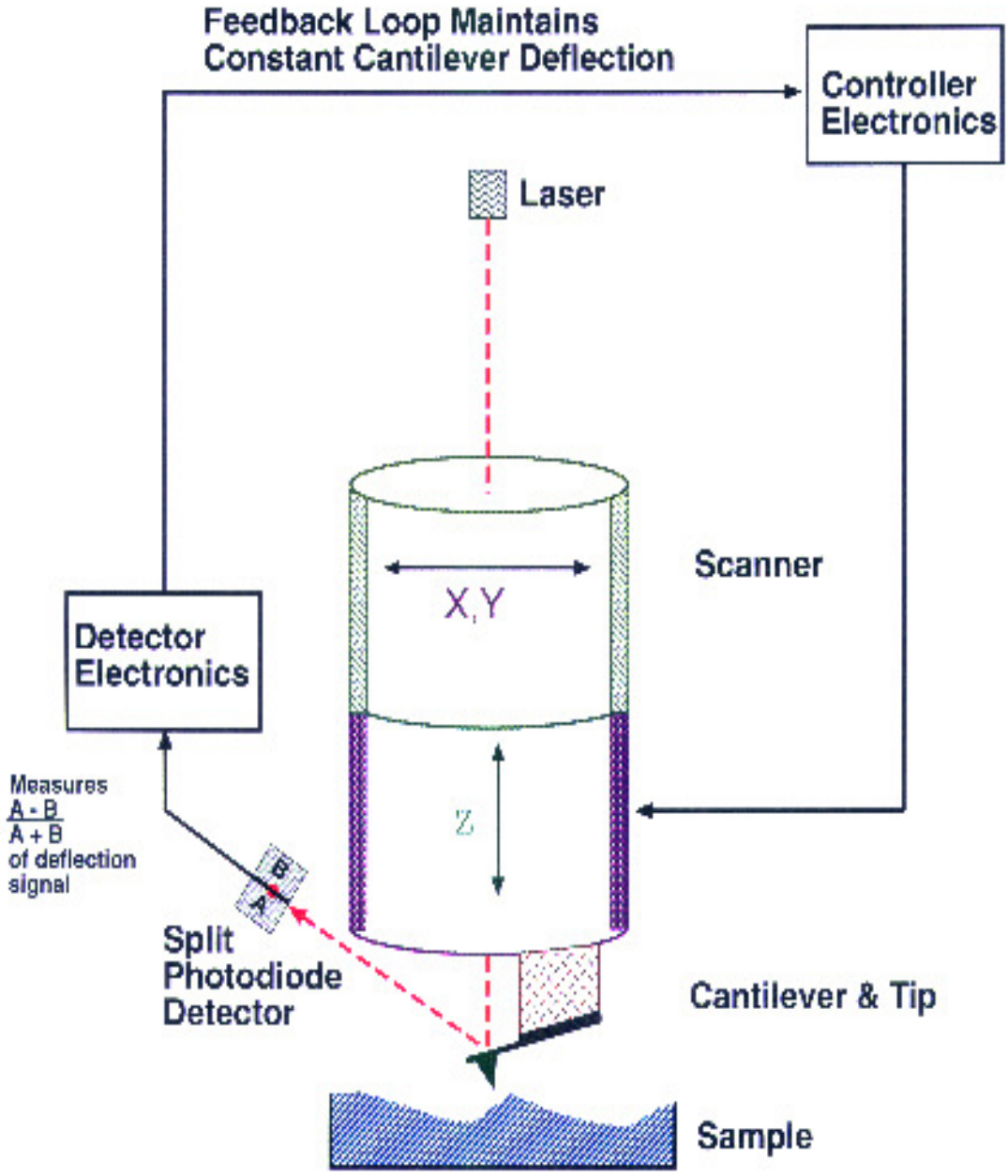

Figure 14 Schematic of a typical AFM machine in contact mode [69]

2.3.2 Scanning Electron Microscopy (SEM)

SEM is one of the most commonly used microscopy technique in material structure analysis. This is because it can provide high resolution image of the material, up to 1 to 5 nm, and clear 2D structure with the microscope's large depth of field. SEM was first developed by Max Knoll in 1935 but the actual SEM machine was actually

built by Sir Charles Oatley and his students from late 1940s to 1965 [70]. The equipment consists of an electron gun that fires the electron beam towards the sample. There are three lenses situated between the gun and the sample, as shown in Figure (15), to focus the laser beam so that its diameter is less than 5 nm, giving the output a much better resolution. The reflected electron beam is then received by the detectors and the detectors are then sending the received information of the substrate topography to the monitor for display.

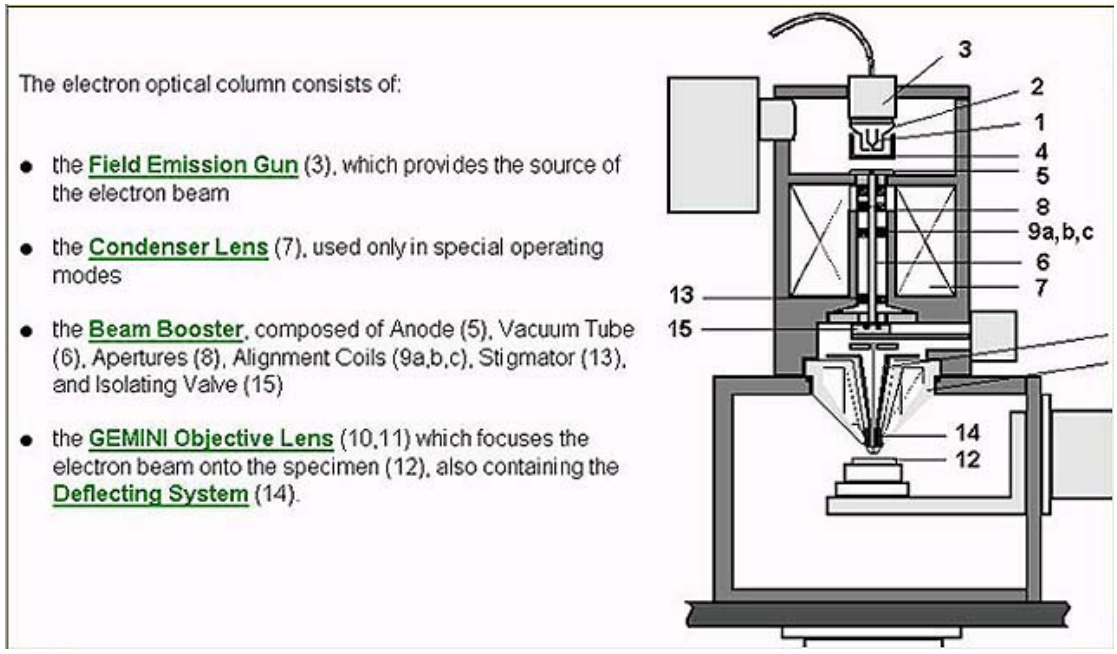

Figure 15 Schematic of SEM structure [71]

2.3.3 Hall Effect Measurement

Thin film material resistivity can be measured using Hall Effect calculation principles. The Hall Effect is the production of the voltage difference across the conductor and the magnetic field that is perpendicular to the electric current that flows through the conductor, as shown in Figure (16).

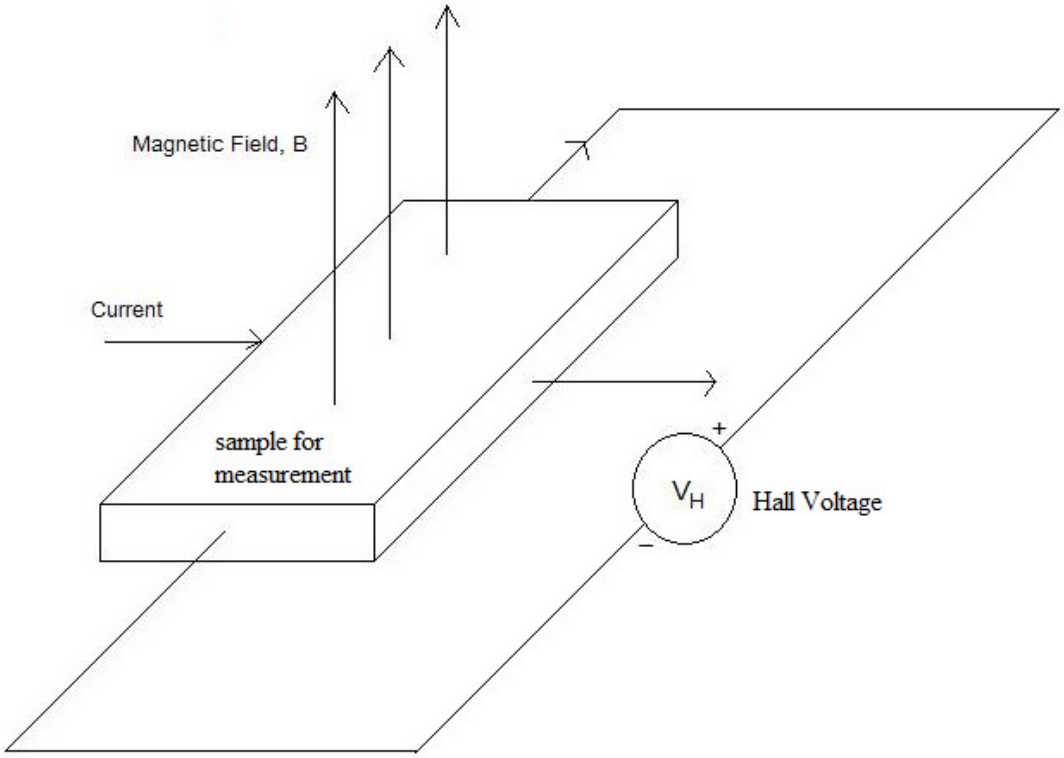

Figure 16 Schematic of hall effect principle showing all the parameters that are relevant to hall effect calculations

Once the Hall Voltage (V_H) is determined, and the current I, magnetic field B and elementary charge q are known, the sheet carrier density, n_s, of the sample can be obtained through the following equation:

$$n_s = IB/q|V_H|. \quad (6)$$

If the thickness d of the material is also known and the sheet resistivity, R_S, is also determined, then the bulk resistivity, ρ, of the sample can be determined by

$$\rho = R_S d. \quad (7)$$

There are several sample geometry choices when operating Hall Effect measurements and the most commonly used one is the Van der Pauaw geometry, developed by Van der Pauaw in 1958 [72]. It uses voltage and current measurements from four contact points of the sample edges to calculate sheet resistance and/or carrier concentration.

This type of geometry can apply to any shapes, as long as there are no holes in the middle. [72, 73]

2.3.4 Spectrophotometry

Spectrophotometry involves the use of a spectrophotometer for measuring optical characteristics. The equipment consists of a spectrometer to produce light of selected wavelengths and a photometer to measure the intensity of the light. Characteristics such as reflectance, transmittance, and absorption are measureable using the equipment. Two identical light beams are produced by the equipment while the photometer records the light intensities that are reflected or penetrated the samples. The basic structure of a spectrophotometer is shown in Figure (17) below. Some of the spectrophotometers would also include a total integrating sphere in the design, as the one used in this research. The sphere is useful especially for reflectance measurements as it diffuses and scatters the incident light uniformly without affecting the light intensity and uniformity. [74]

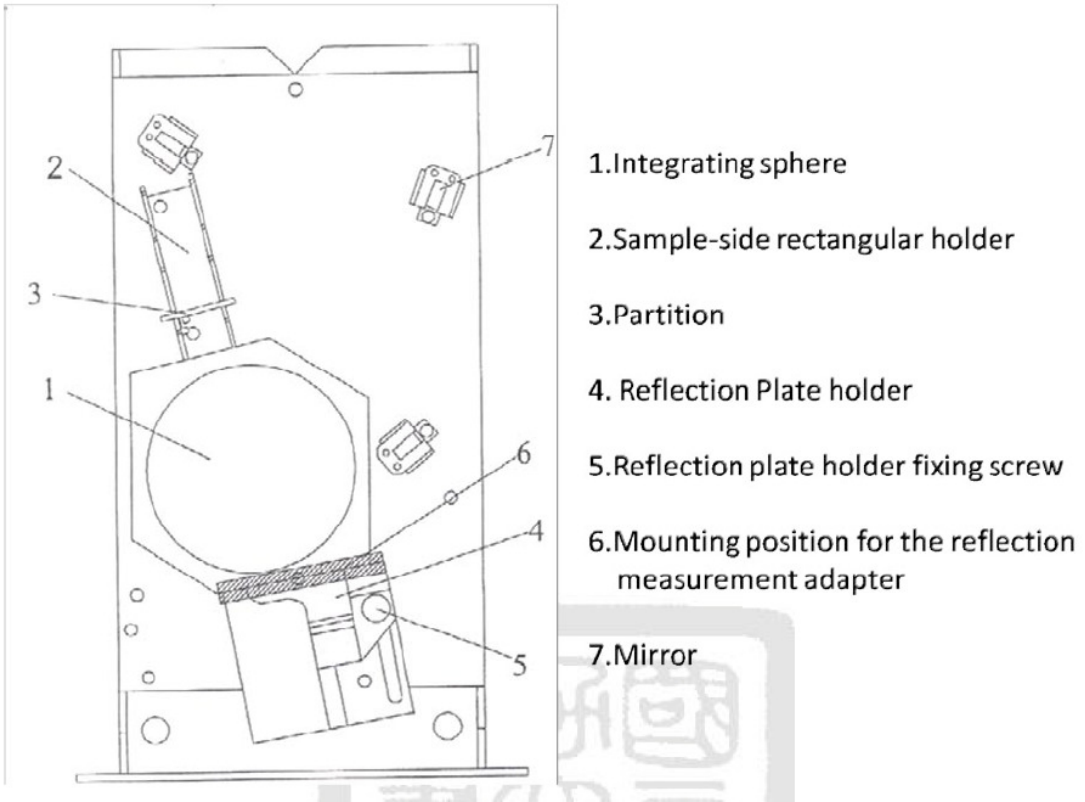

Figure 17 The structure of the spectrophotometry with integrating sphere used in this research [74]

2.3.5 XRD Analysis

Solid materials are formed by atoms or atomic group arranged in certain way. When an x-ray beam is injected into the material, it would be scattered by atoms. If two or more x-ray beams scattered by the atoms that have some phase differences are superimposed onto each other, diffraction is occurred. The x-ray diffraction instrument is used to collect the intensities of the scattered signals to get the diffraction pattern of the measured sample. This pattern is normally as the signal intensity versus the phase angle. When such a pattern is used in the crystal surface calibration process for the sample, the material's crystalline structure, such as the orientation and phase angles, can be obtained. In general, there are two most common ways of processing XRD analysis: GONIO scan and GIXRD. GONIO scan uses the substrate's surface structure to obtain the diffraction signals based on Bragg diffraction theory whereas GIXRD uses grazing angle as incidence angle (normally a 1 ° incidence angle). An advantage for using X- ray diffraction measurement is that it can analyse the material without causing damages on the material. [66]

2.3.6 Solar Simulator System

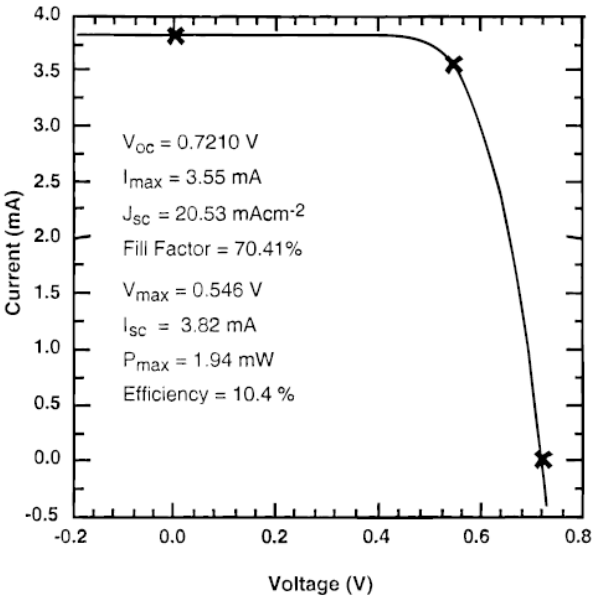

Figure 18 An I-V curve of nearly 11% efficiency achieved by Gratzel's group, showing the maximum power, short circuit current intensity, open circuit voltage and fill factor [27]

To measure the performance of the solar cell, a current-voltage characteristics of a light exposed cell need to be measured and analysed. Such characteristic would provide an I-V curve, such as the one shown in Figure (18), which is normally used for cell conversion efficiency. When a positive voltage is applied to the counter electrode with the cell exposed under the solar simulation system simultaneously, two types of currents can be measured: current formed by the device exposed to solar light like light source and current formed by the forward bias applied to the device. The overall current of the device is the sum of these two currents. If the current is multiplied by the voltage that corresponds with it according to the IV curve, then the power of the device can be obtained. Furthermore, by looking at the IV curve, the maximum power can be determined. If the incident light intensity is known, then the device efficiency is the ratio of the maximum output power and the incident light intensity, as shown in equation (8), where P_m is the maximum output power and P_i is the incident light intensity.

$$\eta = \frac{P_m}{P_i} = \frac{I_{SC} V_{OC}}{P_i} \tag{8}$$

Moreover, the fill factor that corresponds to the quality of the solar cell can be determined as the maximum power value is directly proportional to the multiple of short circuit current intensity, i_{sc}, open circuit voltage, V_{oc}, and fill factor, FF, of the device. The relationship between the fill factor and the maximum power is shown in equation (9).

$$FF = \frac{P_m}{i_{sc} \times V_{oc}} \tag{9}$$

A solar simulator system is commonly used in photovoltaic characterization for efficiency and IV relationship measurements. It uses a light source, normally an arc lamp, which imitates the solar light characteristics, such as light intensity, thermal intensity, in order to create environmental conditions that are similar to the outdoor environments. Most of the simulators in the market work in similar ways except the methods of generating light source, categorizing them into two categories: steady state simulator and pulsed simulator. Steady state simulator generates continuously steady light focus, creating uniform light plane. This type of simulator requires huge amount of energy to maintain the steady state but has simple and cheaper structure. Pulsed simulator, in the other hand, generates short period exposures, resulting in

faster characteristic extractions but a much more complex structure. The simulator's basic structure is shown in Figure (19) below.

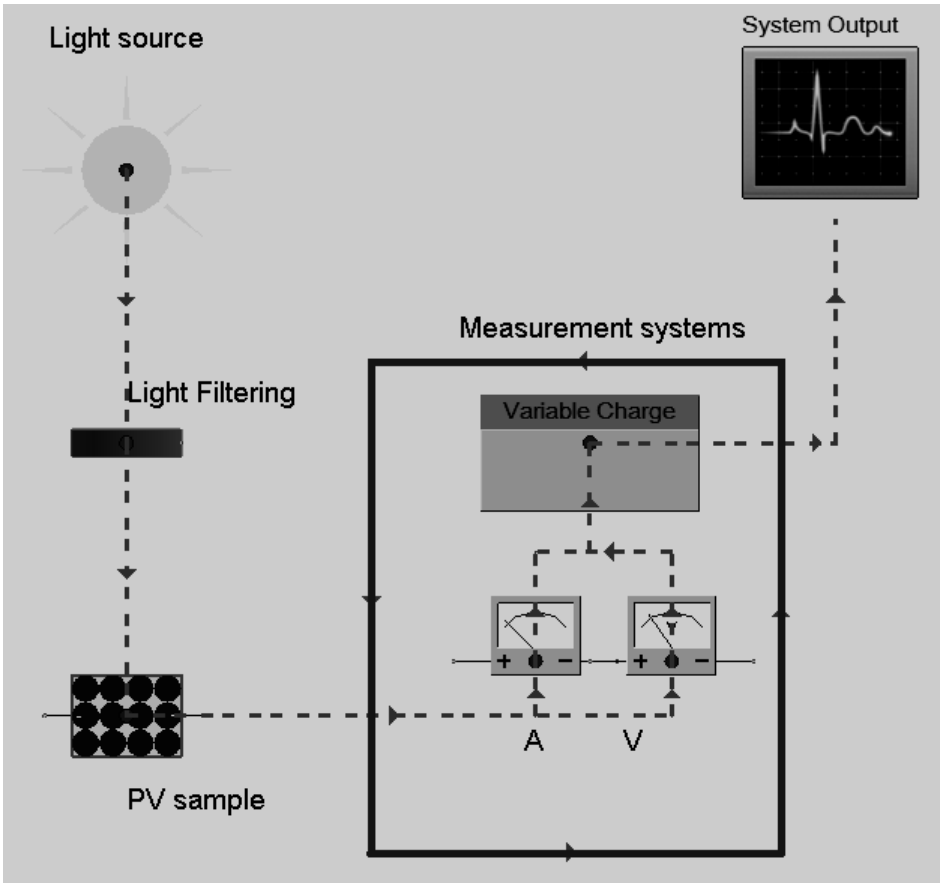

Figure 19 Solar simulator for photovoltaic performance

3.EXPERIMENTAL PROCEDURE

DSSC fabrication involves several essential aspects and can be separated into three categories: substrate surface texturing, transparent conductive oxide layer deposition and cell assembly. This section describes the detailed research procedures on how the DSSC samples are fabricated with textured substrates. Descriptions on fabrication process and analysis process are divided into two different sub-sections: Experimental procedures and Analysis.

3.1 Experimental Plan

The research begins with substrate surface texturing and characterization, followed by Al:ZnO deposition and characterization, and finally DSSC assembly and cell characterization, as shown in Figure (20). Both surface texturing and Al:ZnO deposition are carried out at the nanofabrication Laboratory in Electrical and Electronics Engineering Department, University of Canterbury. The DSSC assembly is done at National Nano Device Laboratory, Tainan, Taiwan.

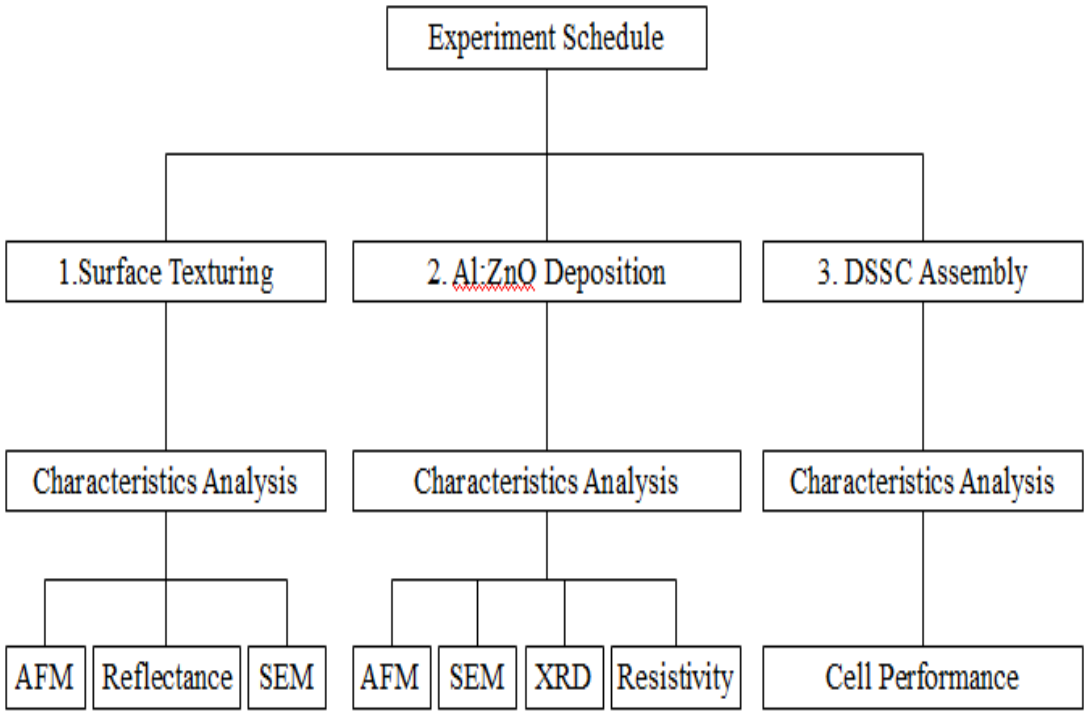

Figure 20 Research plan for surface textured DSSC

3.2 Experimental Equipments

Various equipments were used in this research. Table (1) provides the list of all the important equipments used during fabrication and sample analysis.

Fabrication		
Equipment Name	Brand	Model
Reactive Ion Etcher	Oxford Instruments	Oxford PlasmaLab 80 Plus
RF Magnetron Sputterer	BOC Edwards	Edward A500
Spin Coater		
DC Magnetron Sputterer	Cressington	Sputter Coater 108auto
450 °C Oven		
50 °C Oven		
Hotplate Stirrer	Barnstead/Thermolyne	SP142020-33
Analysis		
Scanning Electron Microscopy	Raith	Raith 150
Atomic Force Microscopy	Veeco Instruments	Digital Instruments Dimension 3100
Hall Effect Measurement System	EGK Corporation	HEM-2000
UV/Vis Sppectrophotometer	Jasco Corporation	JASCO V600
X-Ray Diffraction	PANalytical B. V.	X'Pert PRO MRD
Cell performance and IV Measurement Hardware	ScienceTech Inc	Fully Reflective Solar Simulator SS150W
Cell performance and IV Measurement Software	TELTEC Semiconductor Pacific Limited.	NA

Table 1 Equipments used in the research

3.3 Experimental Chemicals and Materials

Most of the chemicals used in the research are standard chemicals that are normally available in the laboratory. Special materials for DSSC are mostly bought from Uni-OnWard Corp. [75], where NDL engineers normally buy their materials for DSSCs from. Table (2) shows the list of materials used in this research.

Product name	Manufacturer/Brand
ITO glass (7 ohms, 2 cm * 2 cm)	Uni-OnWard
Quartz (2 cm * 2 cm)	Available from the UC nanolab
Microscope Cover Glass (2.2 cm * 2.2 cm)	Available from the UC nanolab
Al:ZnO target	Available from the UC nanolab
TiO_2 P25	Uni-OnWard
Titanium (IV) isopropoxide (97%, Aldrich)	Available from the NDL
absolute ethanol	Available from the NDL
Acetylaceton	Available from the NDL
Triton X-100	Available from the NDL
Dye N719	Uni-OnWard
Ar gas (Zero Grade)	Available from the UC nanolab
N_2 gas (Oxygen Grade)	Available from the UC nanolab
CHF_3 gas	Available from the UC nanolab
Gold (for resistivity measurement contact pad)	Available from the UC nanolab
NiCr (for resistivity measurement contact pad)	Available from the UC nanolab
Iodide/trioiodide liquid electrolyte	Uni-OnWard
Platinum target	Available from the Prof. Lee Laboratory, NCKU
transparent polymer film	Available from the NDL, UC nanolab
deionized water	Available from the NDL, UC nanolab
acetone	Available from the NDL, UC nanolab
methanol	Available from the NDL, UC nanolab
IPA	Available from the NDL, UC nanolab

Table 2 Chemicals and materials used in the research

3.4 Fabrication Processes

This section provides detail description on the recipe of the substrate texturing, TCO layer deposition and cell fabrication process. A flow chart of substrate preparation, including texturing and TCO deposition, is shown in Figure (21). The flow chart of the complete cell assembly process is shown in Figure (22).

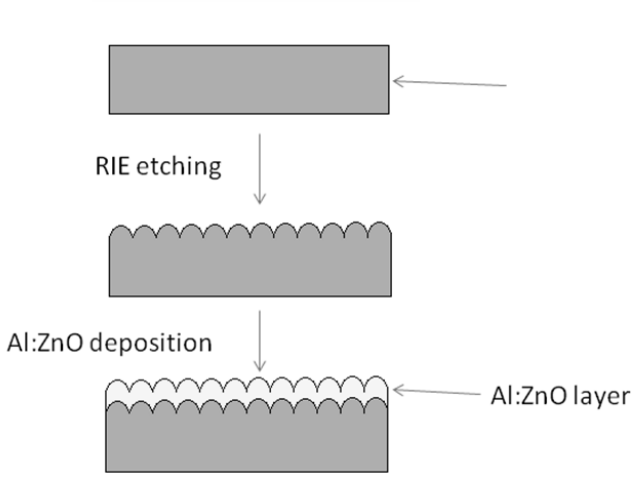

Figure 21 Flow chart of substrate surface texturing and TCO deposition

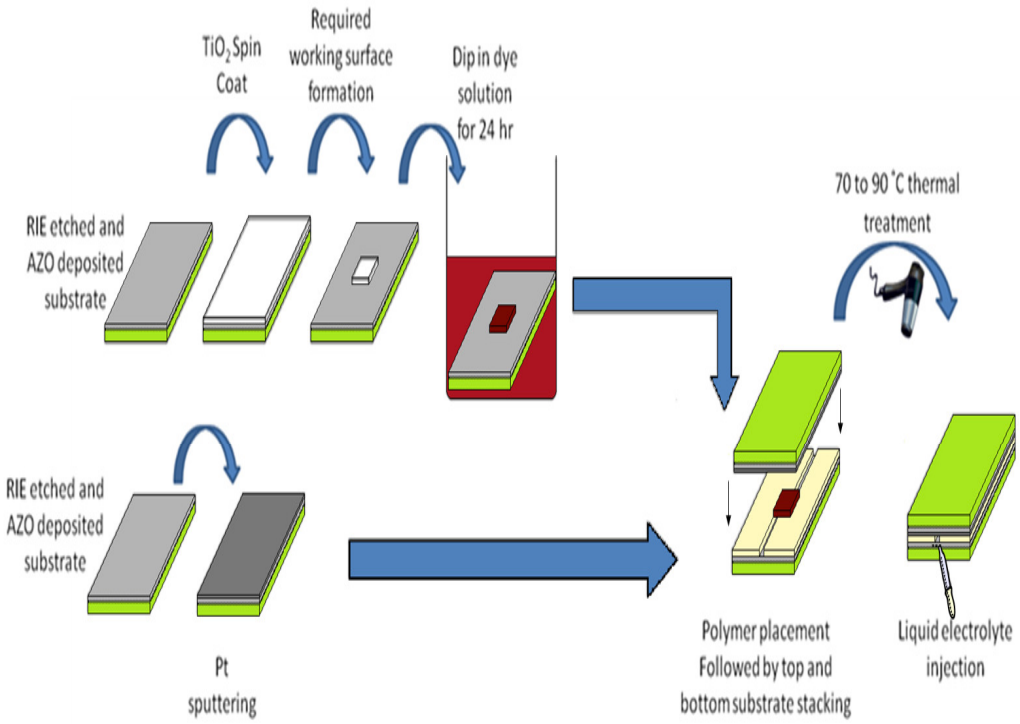

Figure 22 Flow chart of DSSC fabrication

3.4.1 Substrate Cleaning

There are three kinds of substrates being used in this research: microscope cover glass, quartz and industrial Indium doped Tin Oxide (ITO) covered glass. All of the samples have a surface area of approximately 4 cm^2. Apart from the cover glass having a thickness of less than 100μm, the other two types of substrates are around 300μm to 500μm thick. The ITO glass has a layer of 700 μm of ITO with 7 Ω sheet resistances on one side, whereas the other two samples have plain substrates with no thin film pre-deposited.

The substrates are first dipped into Acetone with ultrasonic bath for at least 5 minutes to dissolve unwanted organic materials and to remove dust and contamination material that are left on the substrates post manufacture. Another 5 minutes of ultrasonic bath in Methanol is followed in order to remove the acetone and materials that are not cleansed or dissolved by acetone. Finally, a 5 minute ultrasonic bath in IPA is needed to further remove the residual particles on the substrates. The cleansed substrates are then put inside the 90 °C oven and bake for at least 15 minutes followed by a quick nitrogen blow to ensure that the solvents are vaporized and that the remaining particles are removed.

3.4.2 Substrate Surface Etching

The equipment used in this procedure is Oxford PlasmaLab 80 Plus Reactive Ion Etcher. Previous log sheets of the equipment shows that the most common gases used for glass or quartz dry etchings are CHF_3 and Ar at pressure 0.03 mTorr in room temperature with 25 sccm and 15 sccm respectively. Therefore, the parameters of RIE etchings for this research are based on previous conditions recorded on the log sheets that show good results in glass or quartz etchings.

In order to reduce the fabrication steps, substrates are etched without patterned masks, obtaining random moon surface like morphology on the surface. Samples are test etched in 30 minutes, 60 minutes and 90 minutes in order to get an etch depth that is within the visible wavelength region. Table (3) shows the variations of the conditions in glass etching.

Glass material	laboratory grade cover glass	quartz	-
CHF_3/Ar gas (%)	50/30	50/50	70/30
Time (min)	30	60	90
RF Power (W)	200	-	-

Table 3 Etching conditions for glass RIE etchings

3.4.3 Al:ZnO Deposition

Al:ZnO layer is deposited using RF magnetron sputtering. The equipment used for this fabrication process is Edward A500 developed by BOC Edwards. The RF power is set at 200W with 30 to 40 minutes of ramp up and ramp down. This is to prevent cracking the target from the huge difference in temperature when turning on. The target used in deposition is a 3 inch Al:ZnO, with 2 % of Al_2O_3. Most of the conditions in this work are maintained at constant values shown in diagram (2) except the thickness of the film. Two film thicknesses were targeted in this research—200 nm and 400 nm. 400 nm is approximately the maximum thickness of the film can be obtained using RF sputtering. The substrates are placed in the sputtering chamber with rotation to optimize the uniformity of the film. The thicknesses of the film are confirmed by Dektak thickness measurements. Although it was set at room temperature at the beginning, the temperature changes from 23 °C to approximately 63 °C during the sputtering process.

Power	30 min ramp up from 20Wto 200W and 30 min ramp down to 0 W
Gas	10 sccm Ar gas
Temperature	Varies from 23 °C at the beginning to 63 °C at the end of the process
Duration	1 hr for 200 nm and 2 hrs for 400 nm
Chamber Pressure	$5*10^{-5}$ Pcal
Process Pressure	

Table 4 Parameter settings for RF sputtering

3.4.4 TCO Annealing

Annealing is one of the standard procedures in TCO deposition for improving the electrical characteristics of TCO film. However, for Al:ZnO, there were literatures that demonstrate poor characteristics, giving results of improved electrical characteristics and not improved outcomes.[76, 77] In this experiment, TCO samples annealed at 450 °C for 30 minutes in nitrogen gas is compared with samples that did not go through such process.

3.4.5 TiO_2 Precursor Preparation

TiO_2 precursor is used as a buffer layer between mesoporous TiO_2 layer and TCO layer, as shown in Figure (23). This buffer layer can improve the contact between TiO_2 and the substrates as the precursor can chemically bonds with the TCO coated substrates giving TiO_2 a better stability and less chance of the material got peeled off. Moreover, it acts as a protective layer to prevent the liquid electrolyte to get in touch with TCO layer, resulting in short circuit.

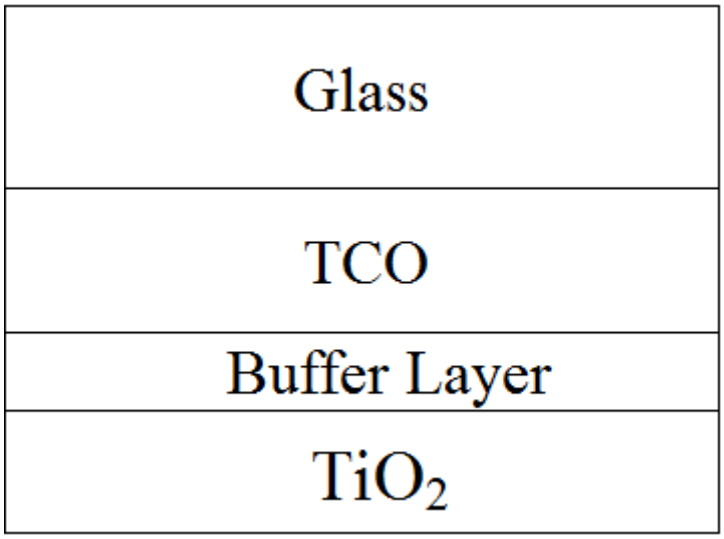

Figure 23 Schematic of the top half of DSSC showing the position of the buffer layer

The recipe of the precursor and the TiO_2 colloid used in this research was kindly provided by the laboratory of Prof. Lee[6], who has been researching in DSSC fabrication for a very long time. The material is prepared, as shown in Table (5), by mixing 30μL of Titanium (IV) isopropoxide (97%, Aldrich), $TiOPr_4$, in 10 mL of absolute alcohol. $TiOPr_4$ needs to be wrapped with aluminum foil to prevent photon bleaching. The solution need to be renewed once it contains white solid substances caused by the mixing of water particles in the atmosphere and the solution.

precursor mixture	
$TiOPr_4$	30 μL
Dehydrated Ethanol	10 mL

Table 5 TiO2 precursor recipe

3.4.6 TiO_2 Preparation

The list of the required material for TiO_2 colloid preparation is shown in Table (6). A long cylindrical bottle is used in preparing the colloid due to the fact that the TiO_2 P25 powder is very light and requires large volume space for 6 g TiO_2 powder. The powder contains TiO_2 particles that are approximately 21 nm in diameter. Moreover, 80% of the particles are in Anatase phase whereas 20% of the particles are in Rutile phase. 10 mL of de-ionized H_2O is then slowly dripped into the middle of the bottle to prevent the mixture to be attached on the container wall. The solution is then stirred using magnetic stirring rod for 2 hours at 50 °C. This is to make sure that the solution is well mixed and that the concentration of TiO_2 colloidal can be maintain at constant value if another bottle of the solution is prepared. The temperature setting produces a slight water vapour that can bring down all the TiO_2 particles that are glued on the bottle's wall. 100μL of Triton X-100 and 200μL of Acetylaceton are then dripped into the solution. Triton X-100 is a very good surfactant that is commonly used as detergents in laboratories. TiO_2 particles are quite sticky since it is in nanometer grade. Triton X-100 can form a layer around each particle so that the particles would not stick back together once it was separated from each other.

Approximately 8 days of ultrasonic bath with constant vibrating frequency is used to

[6] Professor Yuh-Lang Lee: Professor at Department of Chemical Engineering in National Cheng-Kung University, Tainan, Taiwan. He specializes in molecular thin film researches, surface modification and analysis, and colloid and interface chemistry.

properly disperse the particles into the smallest size. In this way, the particles can uniformly dispersed in the solvent, making sure that the particles are well coated with the surfactant to minimize possibility of recombination between two or more particles. The material is extracted using dropper from the surface of the colloid, where the smallest TiO_2 particles are. This is to ensure that the film on each sample substrates would have a similar crystalline structure.

TiO_2 mixture	
TiO_2 P25 powder	6 g
deionized water	10 mL
Acetylaceton	200 μL
Triton X-100	100 μL

Table 6 TiO2 colloid recipe

3.4.7 Colloidal deposition

The TiO_2 precursor and TiO_2 colloidal solution are deposited one after another by spin coating the materials on the substrates using spin coater shown in Figure (4). The acceleration of the spin coating is fixed by the equipment and cannot be measured. The layers are deposited at 800 rpm for 20 seconds, giving a thickness of approximately 2 μm for each layer and 8 μm for the total TiO_2 film. One layer of precursor is deposited first, followed by 4 layers of colloidal solution when the precursor layer is dried under room temperature. However, due to the fact that the colloidal solution condition can be greatly affected by the humidity and temperature of the environment, occasionally only 3 layers of TiO_2 solution is needed if the solution appears to be much thicker than usual. Much thicker film may create cracks on the surface, resulting in huge resistivity on the surface.

30 minutes of 50 °C soft bake is required in between the TiO_2 layers to make sure the layers are dried and solid so that there are gaps in between the layers for much better dye absorption. Multi-layers of TiO_2 are used in DSSC fabrication because dye particles can be absorbed much faster and more dye particles can be directly attached to the surface of TiO_2 particles.

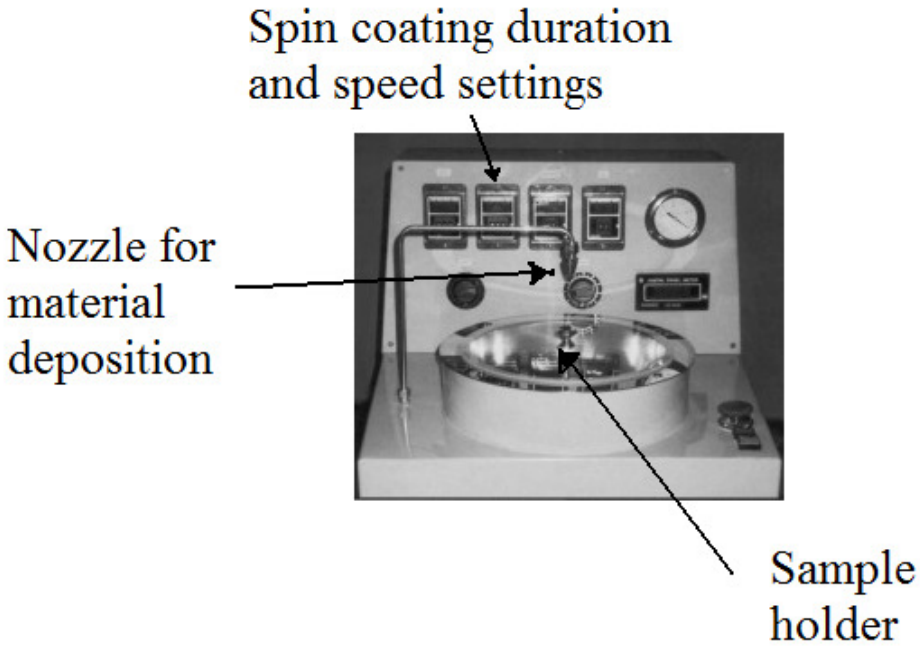

Figure 24 Spin coater used for TiO_2 colloid spin coating—sample holder holds the sample by using vacuum pump and the settings are set at 800 rpm for speed and 20 seconds for duration.

3.4.8 Heat Treatment

Before the heat treatment, the already dried TiO_2 layers are cut into 0.16 cm^2 using scraping knife, as shown in Figure (25). The excess area is cleansed by ethanol. 30 minutes at 450 °C heat treatment is required after TiO_2 material deposition. This is to ensure that the polymer or macromolecules in TiO_2 colloid such as Acetylaceton, can be removed, leaving tiny holes in TiO_2 layers, resulting in better dye absorption and better contact between TiO_2 particles. In consequence, it optimizes the chances of electrons being excited by the photons and increases the amount of excited electrons entering TiO_2 conduction band. The process begins with a temperature ramp up of 6 hours in case a rapid change in temperature gives a condition change in TiO_2 surface crystalline structure. It also ends with a natural temperature ramp down of approximately 1 °C per minute for optimizing cell performance. The high temperature oven used in this research contains a digital setting that can preset the time required to reach a certain temperature and the length of time to maintain in that temperature level.

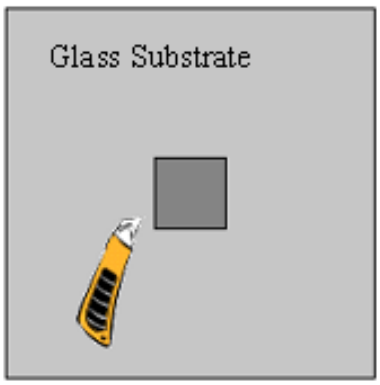

Figure 25 Active working area (0.16 cm^2) formation using scrape knife

When the temperature has dropped below 80 °C, the samples need to be removed from the oven and placed inside the prepared dye solution. Hard baked TiO_2 samples could only be stored either inside the vacuum environment or at 50 °C oven for overnight if the rest of the fabrication steps cannot be processed on the same day.

3.4.9 Dye Solution

The dye solution used in this research is N719, a red wine colour solution commonly used in DSSC laboratories. The material is normally available in powder form from commercial companies and dissolved in chemicals before use. The dye solution used in this research is already prepared by other members in NDL laboratory prior to the launch of this research. Therefore, the exact recipe of dye solution is unknown. The samples need to be fully covered with dye solution for 16 to 24 hours under 50 °C for the dye particles to be fully absorbed. Due to the fact that N719 is a light absorbing material, it needs to be store in the dark, preventing the loss of functionality. The samples need to be rinsed with ethanol and a quick nitrogen blow when taken out from the solution to remove the excess dye solution.

3.4.10 Platinum Counter Electrode Deposition

The material chose for counter electrode is Platinum since Pt has good reflectivity and good conductivity. It was deposited using DC sputter (Cressington Sputter Coater 108auto) at room temperature with current 40mA for 105 seconds to get approximately 25 nm thick Pt film on pre-cleaned TCO deposited substrates. Samples need to be placed at the centre of the chamber as the outer rim of the stage may not receive sputtered Pt material.

3.4.11 Cell Assembly

Two substrates—one with TiO_2 deposition and one with Pt coating, are stacked together face to face. Because surface textured substrates can be used on top or bottom DSSC substrates, several ways of stacking have tried out. Diagram (7) shows the ways of cell stacking used in this research

Front contact	back contact
ITO	STG
ITO	Q
ITO	AIG
STG	ITO
STG	STG
AIG	AIG
Q	ITO
ITO	PG
PG	PG
PG	ITO

surface textured glass=STG
plain glass=PG
Quartz=Q
AZO + ITO = AIG

Table 7 list of materials used as front and back substrates for DSSC cells.

Two pieces of transparent spacers with approximately 60μm thick are placed between the substrates to isolate the working space and prevent short circuit between the positive and negative contact pads when the liquid electrolyte is injected. The assembled sample is then heated at 70 °C to 80 °C for a short period to soften the spacer so that the top substrate and the bottom substrate can be firmly attached together. The spacers are placed and shaped as shown in Figure (26), leaving a channel for electrolyte injection. A hair blow dryer is used instead of the hotplates or oven is that it can rapidly heat up the spacer and can provide uniform thermal proximity to the sample. It is used instead of a hotplate because it can provide a better temperature consistency for the environment around the cell. Once the cells are properly assembled, the liquid electrolyte (tri-iodide) is then injected into the sample before solar cell performance measurement. The liquid electrolyte dries out fairly fast when it is in with the air, especially when the injected amount is so little, less than 100 μL, it is necessary to do the measurement straight after tri-iodide injection.

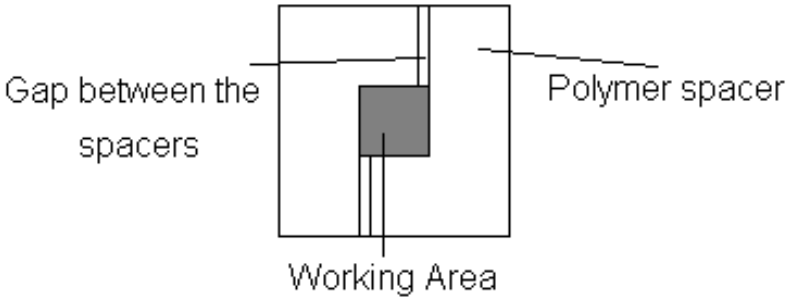

Figure 26 Geography of placing transparent polymer spacers

3.5 Analysis

The following analysis techniques are used in DSSC device, TCO film and substrate surface texturing characterizations. The basic operation principles of each characterization techniques are described in chapter 2. This section gives a brief description on the parameter settings of the techniques used in this research.

3.5.1 SEM Analysis

SEM images of substrates at different fabrication processes were taken using Raith 150, equipment that can be used for both electron beam lithography and SEM. The microscope lens is set at 5k or 30k times magnification. The voltage was set at 10 kV and the working distance was set at 6 mm.

3.5.2 AFM Analysis

The AFM in the laboratory is Digital Instruments Dimension 3100 developed by Veeco Instruments. It has three modes of operation for AFM analysis and tapping mode is the one used in this research. The cantilever tips used in this process are developed by Budget Sensors. The scanning sizes are mostly set at 10 μm and occasionally at 1 μm for a zoom in surface topography. By using AFM to scan the substrate surfaces, three characteristics of the substrates are obtained: surface roughness, surface etched depth and the overall surface texture pattern.

3.5.3 Reflectivity and Transmission Analysis

Both reflectivity and transmission of the substrates are measured using JASCO V600 UV-Vis/NIR Spectrophotometer developed by Jasco Corporation. The measuring wave length is set from 200nm to 2000 nm. An Integrated Sphere is used for reflectivity analysis. This is an essential part for the measurement due to the fact that it makes sure that all the incidence lights are all gone to the sample, improving the accuracy of the measurement.

Figure 27 UV-Vis Spectrophotometer used in this research [78]

Some of the substrates were test measured using a simple set up of spectrometer used in Physics department, University of Canterbury, before going to Taiwan for the second part of research. However, due to the fact that the set up could only collect the reflected light from certain angles, the measurements obtained are not really accurate.

3.5.4 XRD Analysis

The equipment used for XRD analysis is X'Pert PRO MRD developed by PANalytical B. V., available in National Nano Device Laboratory, Hsingchu, Taiwan. Its x-ray is sourced from copper target with $\lambda = 0.154$ nm and the beam size is around 20 mm height with 3 mm width. Figure (28) shows the image of the equipment.

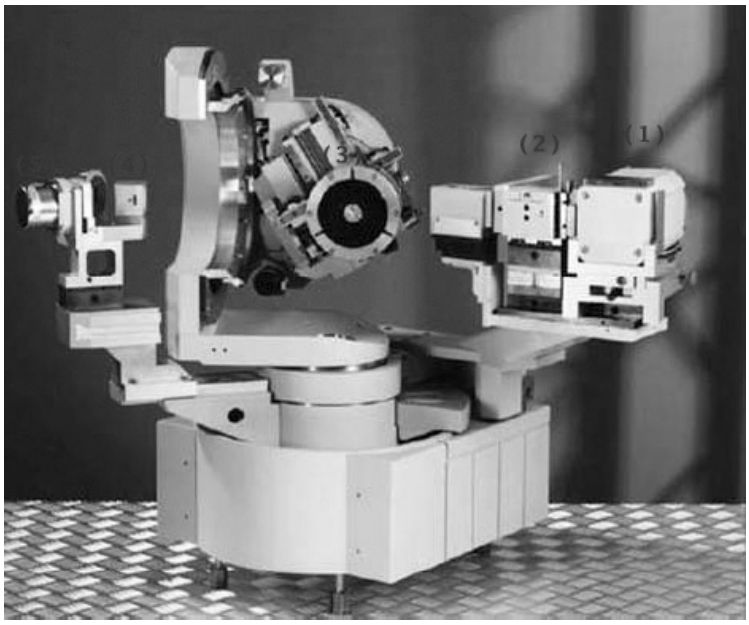

Figure 28 Image of the XRD equipment: (1) X-ray tube, (2) Primary optical module, (3) Sample cradle, (4) Secondary optical module and (5) Detector

3.5.5 Resistivity Analysis

The resistivity of the substrates that are coated with Al:ZnO were measured and compared with that of ITO. The method used in this research for resistivity analysis is the Hall Effect measurement, using EGK Hall Effect measurement system, as shown in Figure (29).

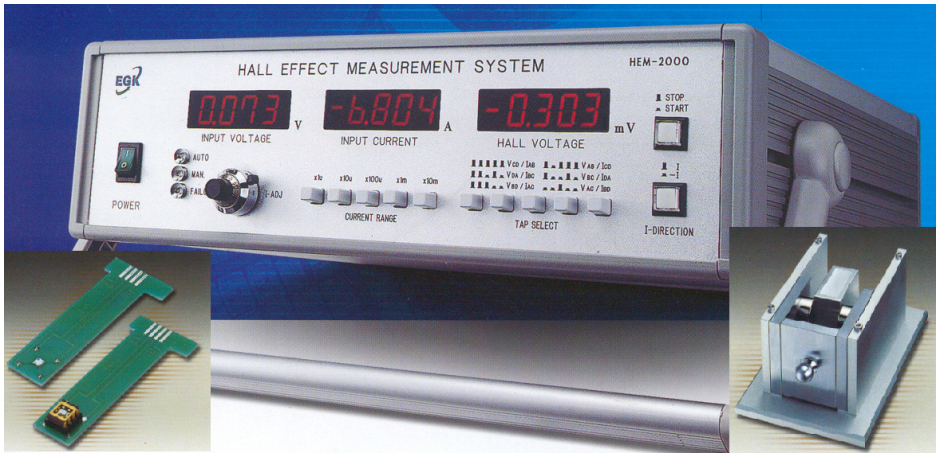

Figure 29 Image of EGK Hall Effect measuring system [79]

3.5.6 Solar Cell Efficiency Analysis

The assembled cells are analyzed using Fully Reflective Solar Simulator 150W developed by ScienceTech Inc. and the accompanied IV measurement software developed by TELTEC Semiconductor Pacific Limited, as shown in Figure (30). This simulator produces high intensity and uniform illumination on a target area with specially designed mirrors that "fold" the light towards the target, resulting in reduced the light losses and eliminated the spectral distortion. The equipment can simulate various sun light conditions, including sea levels and in outer space [80].

Figure 30 ScienceTech Fully Reflective 150W Solar Simulation System [80]

The light source for this experiment has an intensity of 1 SUN, which is 100mW/cm^2, for a target size of 25 cm^2 and the type of filter used for the simulation system is Air Mass 1.5G (AM 1.5G). The filter is used to adjust the system's light source so that

the light source can imitate sun light at different conditions. AM 1.5G provides light source that is similar to the sun light at sea level and takes into account of the radiations that are both directly from the sun and reflected back to ground by the sky or the sea. [81] The temperature is controlled at 25 °C, a standard equipment default setting. The voltage range for IV measurement is from -1 V to 1 V in steps of 0.1 V. The cell is placed on the simulator stage as shown in Figure (31), where the positive plug is connected to the Pt side and the negative probe is connected to the other substrate with TiO_2.

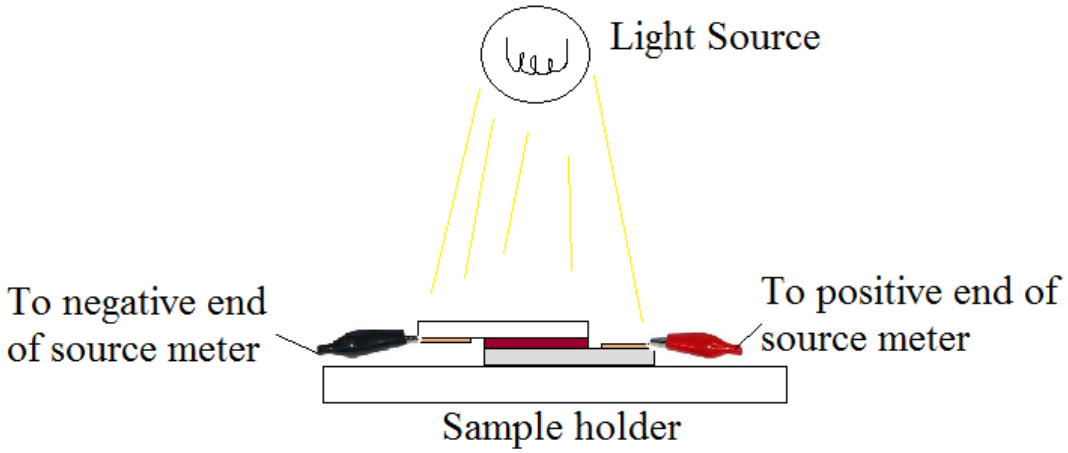

Figure 31 Cell placement on solar simulator: clear side face up

4. Results and Discussion

4.1 Substrate Surface Texturing

Irregular lumps were formed on the substrate surfaces after etching as shown in Figure (32). The reason for the formation of these lumps is due to different etching selectivity and it is most likely due to the composition of the material. Cover glass substrates are usually silicate or borosilicate glass which contains mainly SiO_2. CHF_3 gas reacts with SiO_2 and forms CO, SiF_4 and H_2 gases. There are also other materials in the glass composition that do not react with CHF_3 gas and thus create this moon like surface pattern. The substrate was etched to approximately 400 nm deep, with roughness around 100 nm, as shown in Figure (33) and Figure (34). Quartz substrates are also used in the experiment but the substrates showed no sign of etching with the same gas mixture. According to literatures, this may be because of the material composition and the thickness of the substrate [82, 83].

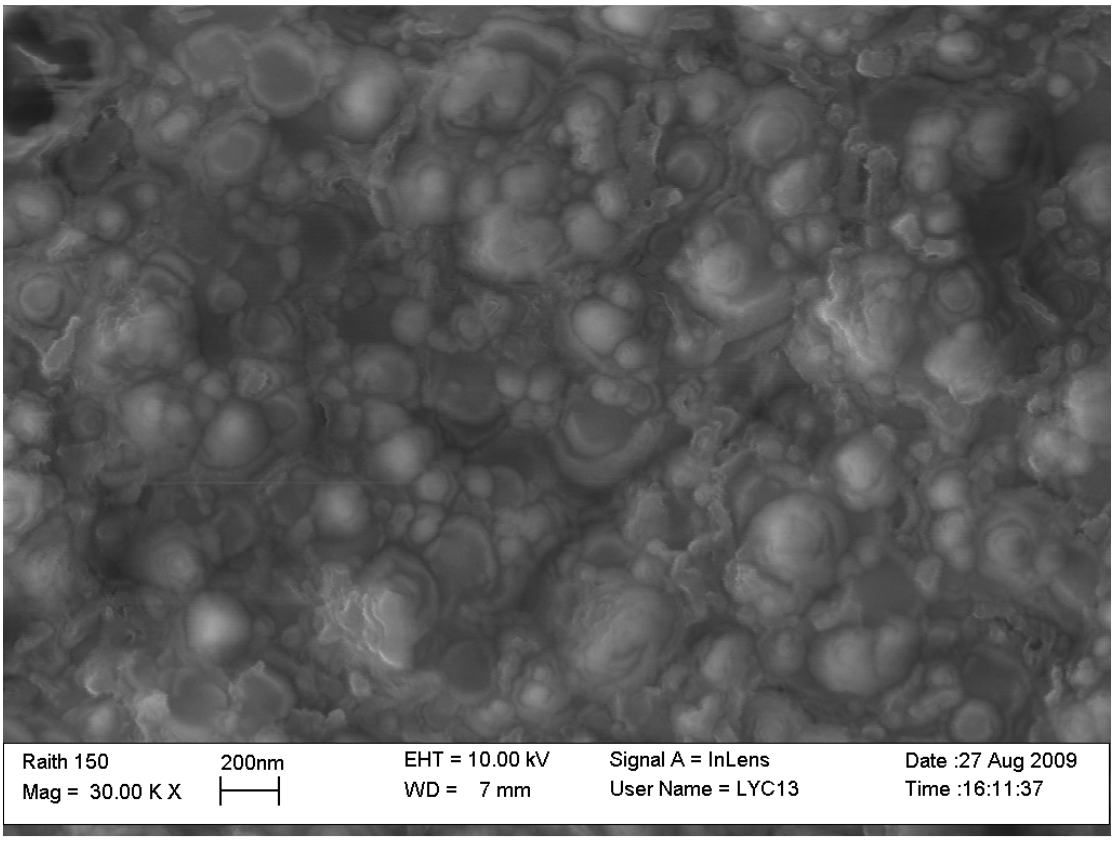

Figure 32 SEM image of 1 hour RIE textured glass

The roughness of the surface is approximately 80 nm. The roughness of the substrate is important because it helps to improve the light scattering in the cell and increases the actual effective area for the cell.

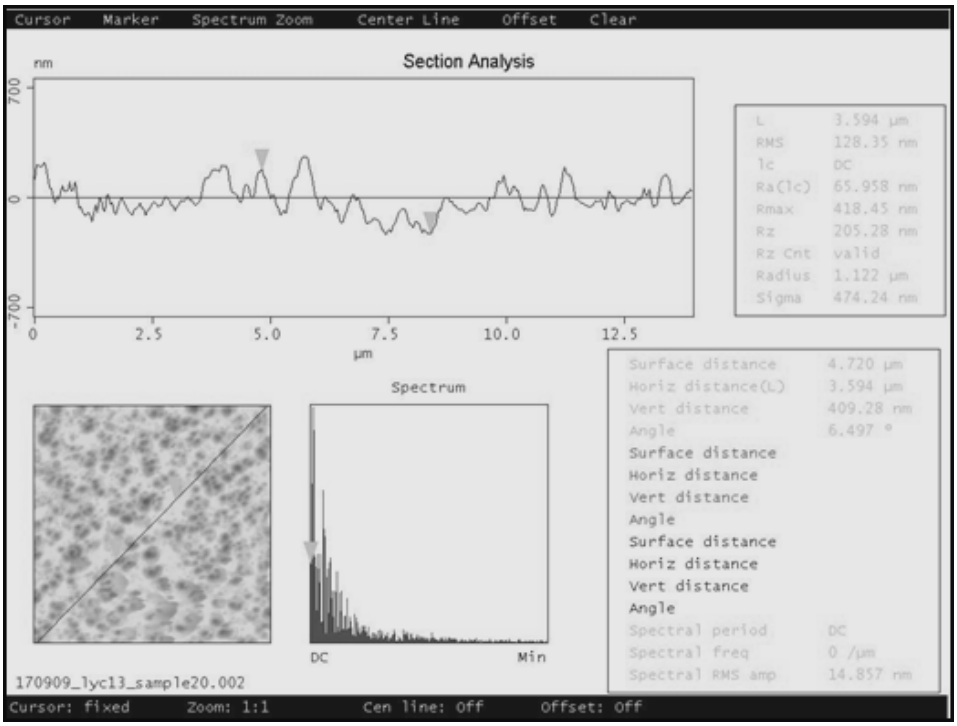

Figure 33 AFM image of 1hr RIE etched sample, showing the etch depth of around 400 nm

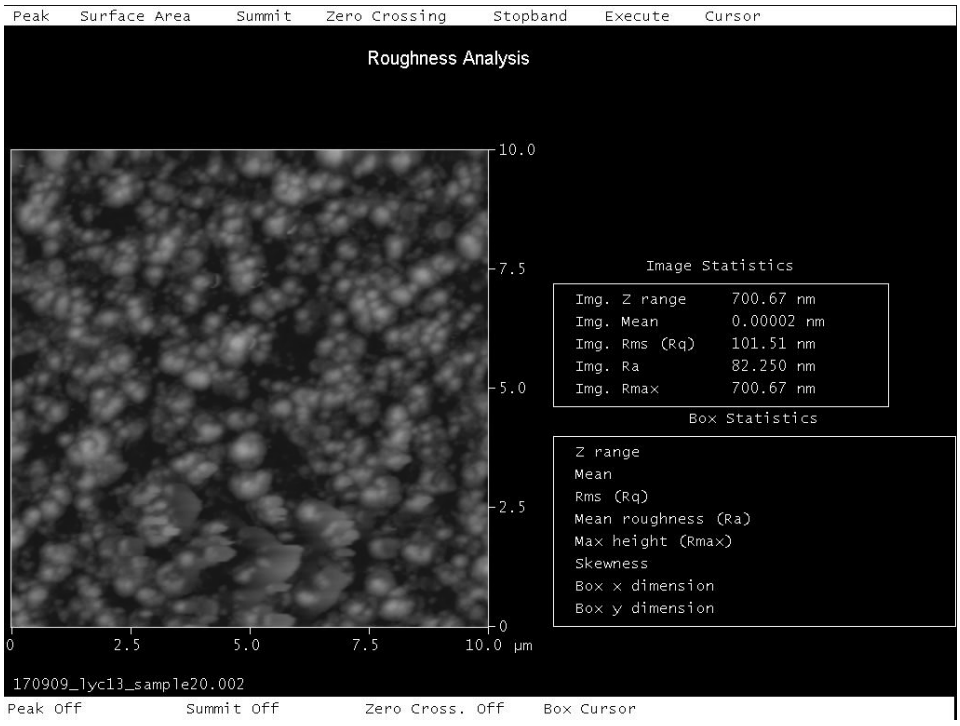

Figure 34 AFM image of 1hr RIE etched sample showing the surface roughness profile

Figure (35) shows the reflectance comparison of the 1 hour RIE etched substrate with the unprocessed substrate. There is a significant drop in reflectance after RIE etching, especially for wavelengths above 500 nm and for near UV region. Because an integrating sphere was used in the measurement, light waves from all incident angles are considered.

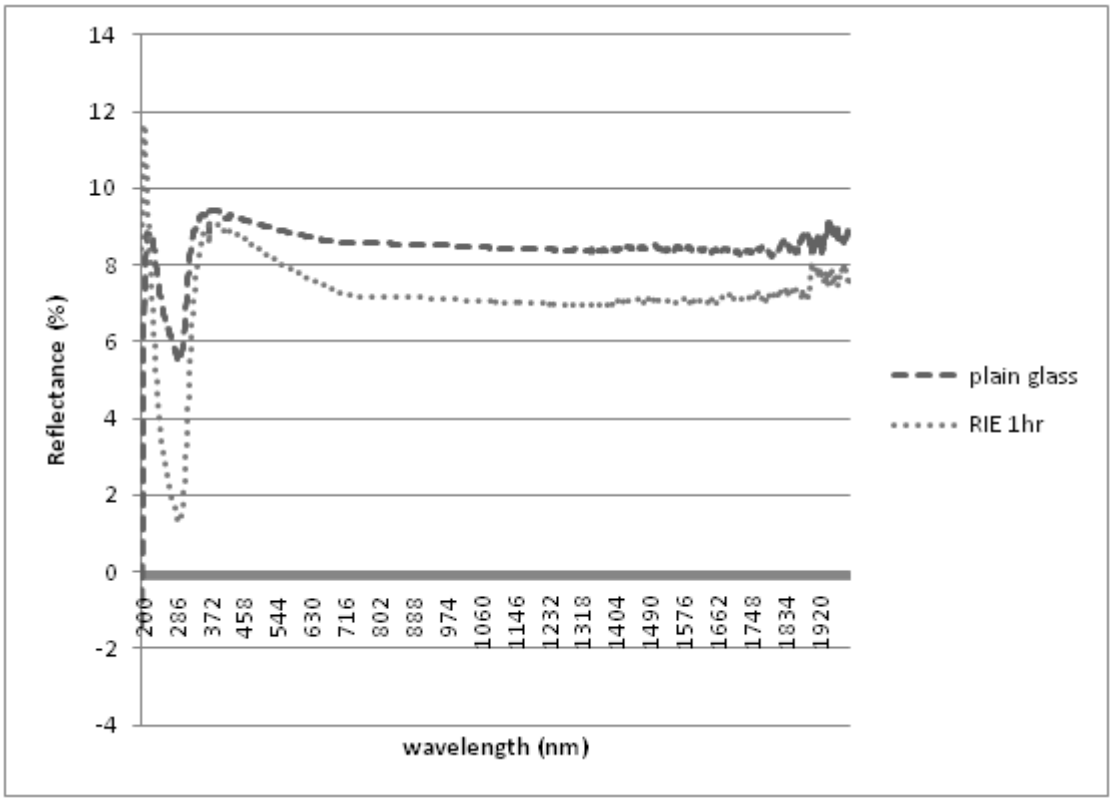

Figure 35 Reflectance of the textured substrate compared with the plain glass

4.2 Al:ZnO Deposition

After Al:ZnO deposition, a flower buds like structures are formed on the substrate surfaces. The sputtered Al:ZnO material, although uniformly deposited, tends to distribute more on the hills of the etched substrate surface instead the valley. Figure (36) shows the SEM result for the RIE etched substrate surfaces with Al:ZnO layer. SEM image was also taken for Al:ZnO deposition on non textured substrates, as shown in Figure (37). The film lies on the surface along the substrate and none of the material grows in perpendicular direction to the substrate surface.

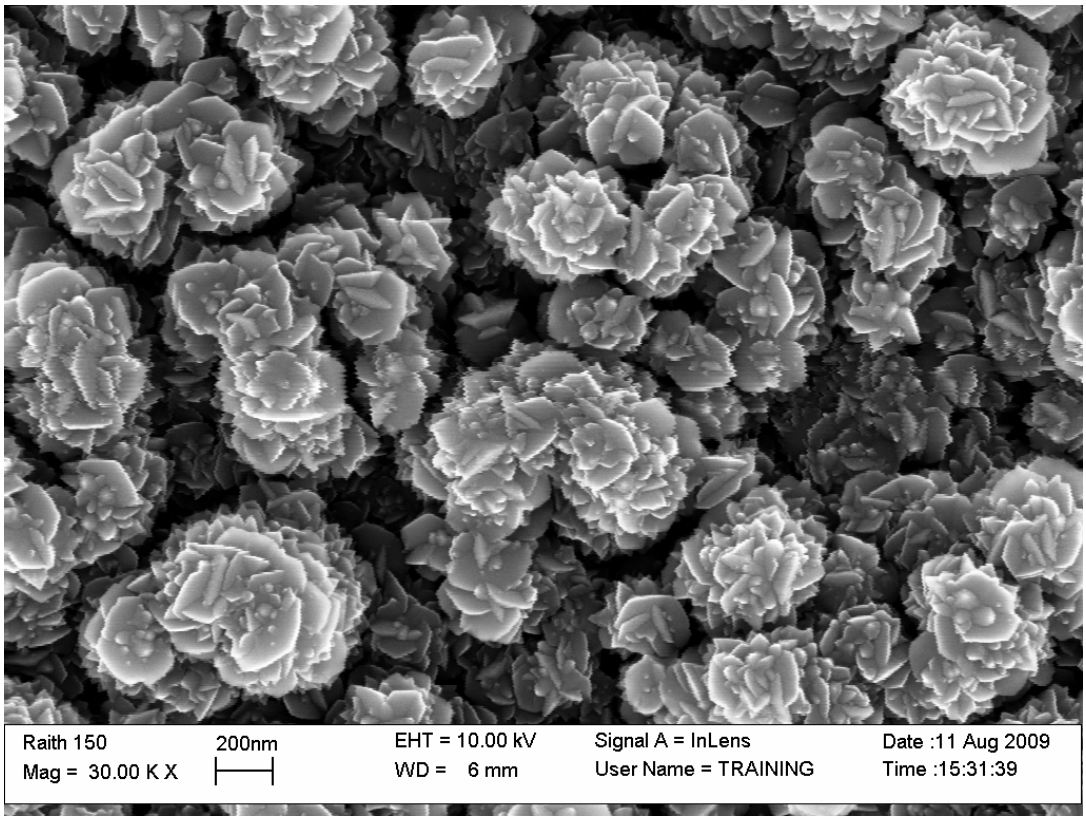

Figure 36 SEM image of 200nm thick Al:ZnO deposited on a surface textured substrate

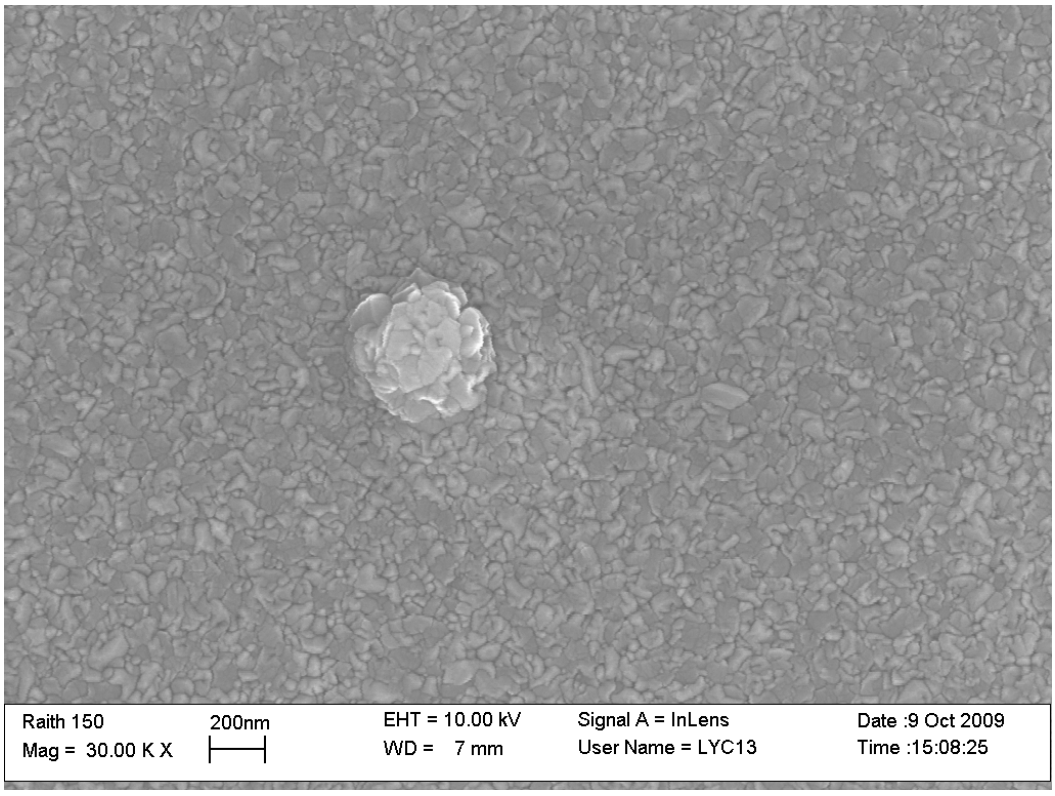

Figure 37 SEM image of 400nm thick Al:ZnO deposited on a non-textured substrate

The reflectance of Al:ZnO film is also measured and compared with film deposited on untextured substrates and textured substrate with no Al:ZnO deposition, as shown in Figure (38) and Figure (39). The deposition of Al:ZnO has caused the reflectance to increase to approximately 20 to 25 %, similar to the one mentioned in the paper published by A. V. Singh *et al*.[84] The reflectance at certain wavelengths has even increased to approximately 25%. However, when it is deposited on RIE etched substrates, a dramatic decrease in reflectance for wavelength above 700 nm is observable. The maximum reflectance was decreased from 25% to 20% at approximate 400 to 500 nm wavelength range. Further investigations such as modifying the etching recipe to obtain low reflectance at visible wavelength can be done in the future to improve the result.

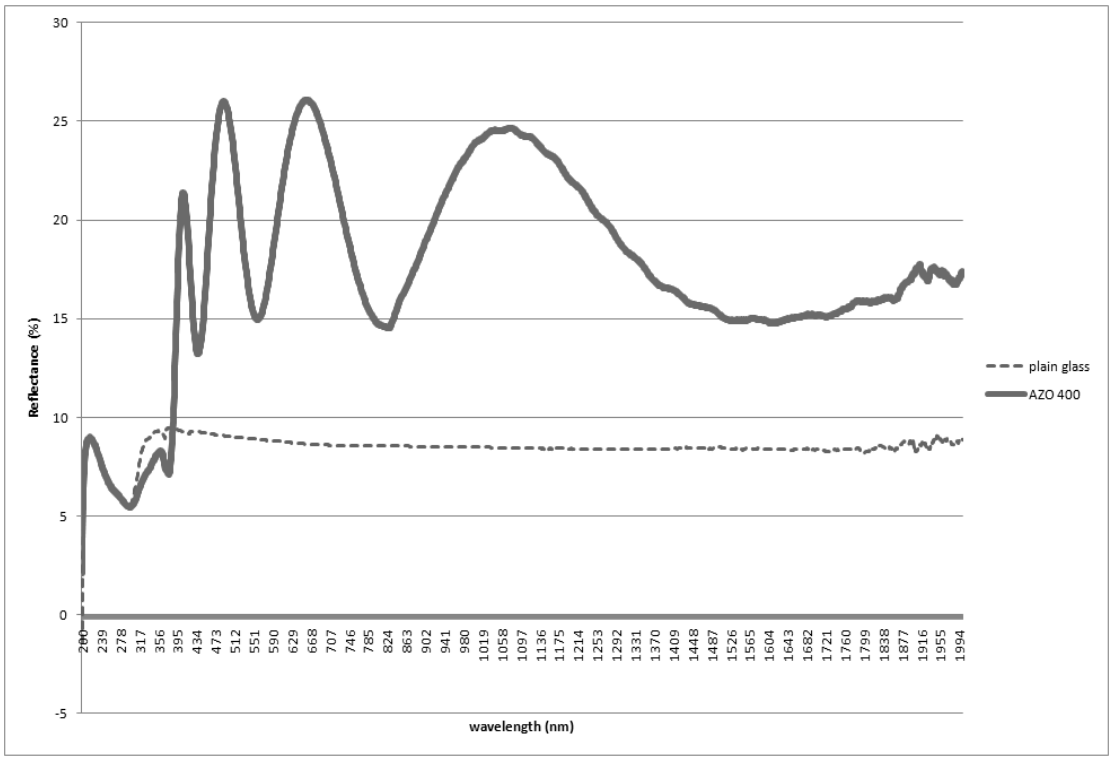

Figure 38 Reflectance comparison between plain glass and 400 nm thick Al:ZnO film deposited on un-textured glass

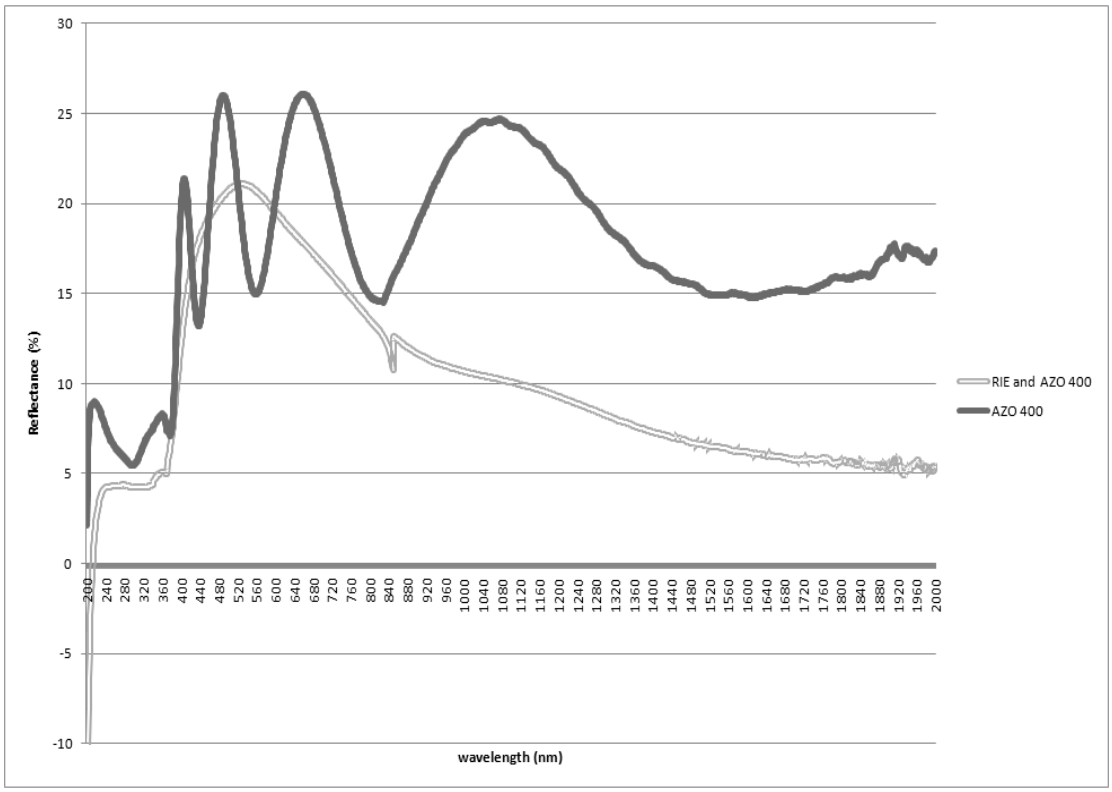

Figure 39 Comparison of reflectance of 400 nm thick Al:ZnO deposited on plain glass and on surface textured glass

The resistivity of the film was initially test measured using Hall Effect equipment. The measured values are much higher, 7 KΩ, compared with ITO on glass has a 7 Ω sheet resistance. The resistivity of AZO film measured are shown in Table (8).

Substrate type	Film thickness (nm)	Resistivity (Ω.cm)
textured glass	200	0.024
textured glass	400	0.00312
untextured glass	200	0.054
untextured glass	400	0.016

Table 8 resistivity measured from the substrates

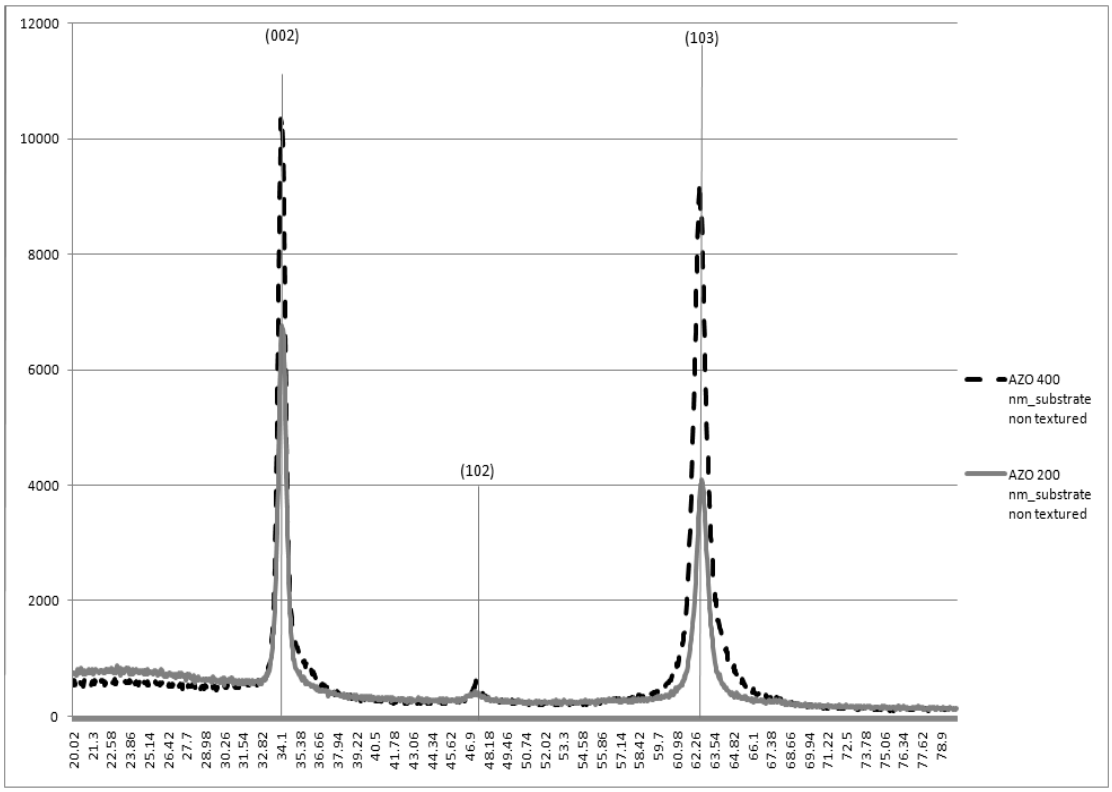

Figure 40 XRD comparison between 400 nm thick AZO and 200 nm thick AZO

Because of the high resistivity measurement and high reflectance value, the deposited film was also measured in XRD to see the material's crystalline structure and compare it with literatures [85]. Figure (40) shows the intensities of the x-ray signals of different AZO thickness reflected at various phase angles. With AZO deposited on non textured cover glass, (002) and (103) peaks show high intensity at 34 ° and 62.3 ° phase angles respectively. The high intensity of (002) and (103) show an oriented growth of the film on along the *x,z* plane that is perpendicular to the substrate surface. The thickness of the film only affects the intensities of the peaks, indicates a more directional crystalline structure in thicker film. When the film is deposited on textured glass, a different result, such as the one in Figure (41) was obtained. There are several different intensity peaks that are not in the AZO film deposited on plain glass. The presence of peaks (101), (110), (102), and (101) in the pattern is similar to the undoped ZnO crystalline orientation presented by Mondal et al. [86], a typical pattern of a hexagonal ZnO structure. This would mean that the AZO film on the textured substrate shows more of the ZnO hexagonal crystalline structure compared with the film deposited on the non-textured glass.

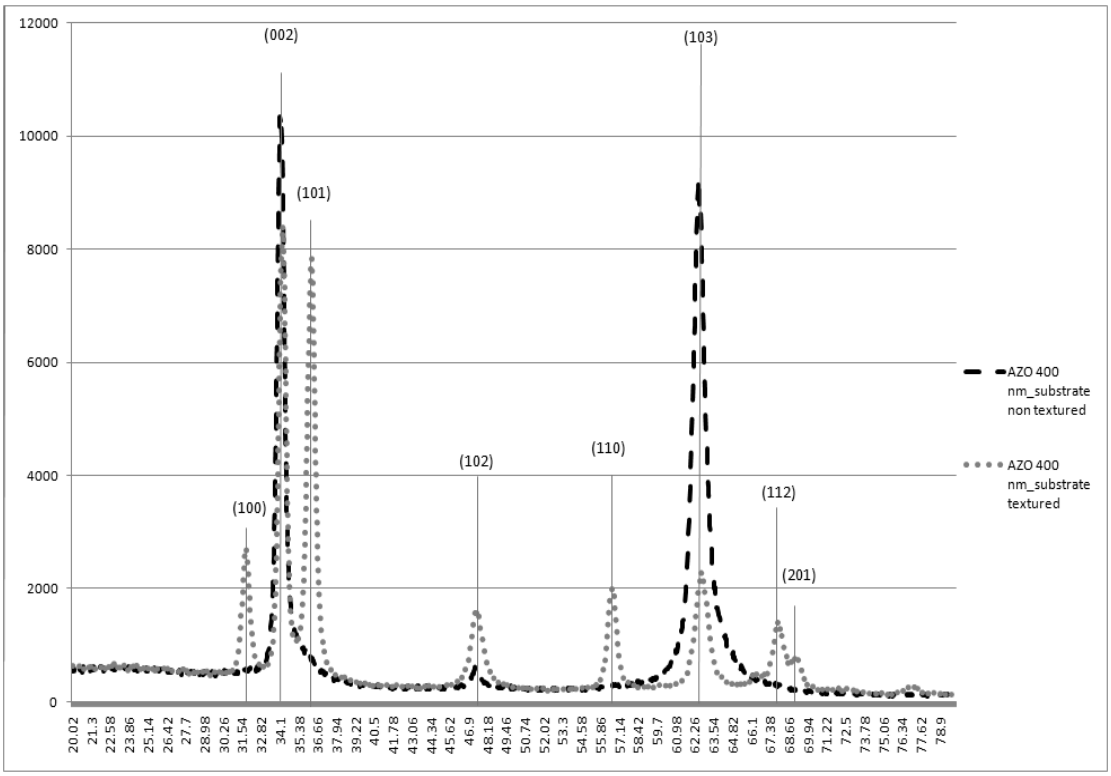

Figure 41 XRD comparison for 400 nm of AZO deposited on plain glass and surface textured glass

4.2.1 Al:ZnO Annealing

Some of the AZO coatings on textured glass samples were test annealed at 400 °C for 30 minutes with nitrogen gas flowing through the chamber. The resistivity of the samples has increased rapidly after annealing to 400 °C. Table (9) shows the resistivity values of the samples before and after annealing. SEM image of the film after annealing indicates no apparent changes in crystalline structures, as shown in Figure (42) and Figure (43). According to the Lin [77], the increase in resistivity is because of nitrogen being chemically absorbed onto the surface of the film and into the crystalline structure, resulting in the distortion of the lattice. In consequence, it decreased the film's carrier mobility to less than 5 cm^2/VS and thus affects the resistivity of the cells to the values in Table (9).

Film Thickness (nm)	Resistivity before annealing (Ω cm)	Resistivity after annealing (Ω cm)
200.00	0.07	0.20
300.00	0.27	4.40

Table 9 Resistivity values increases after annealing

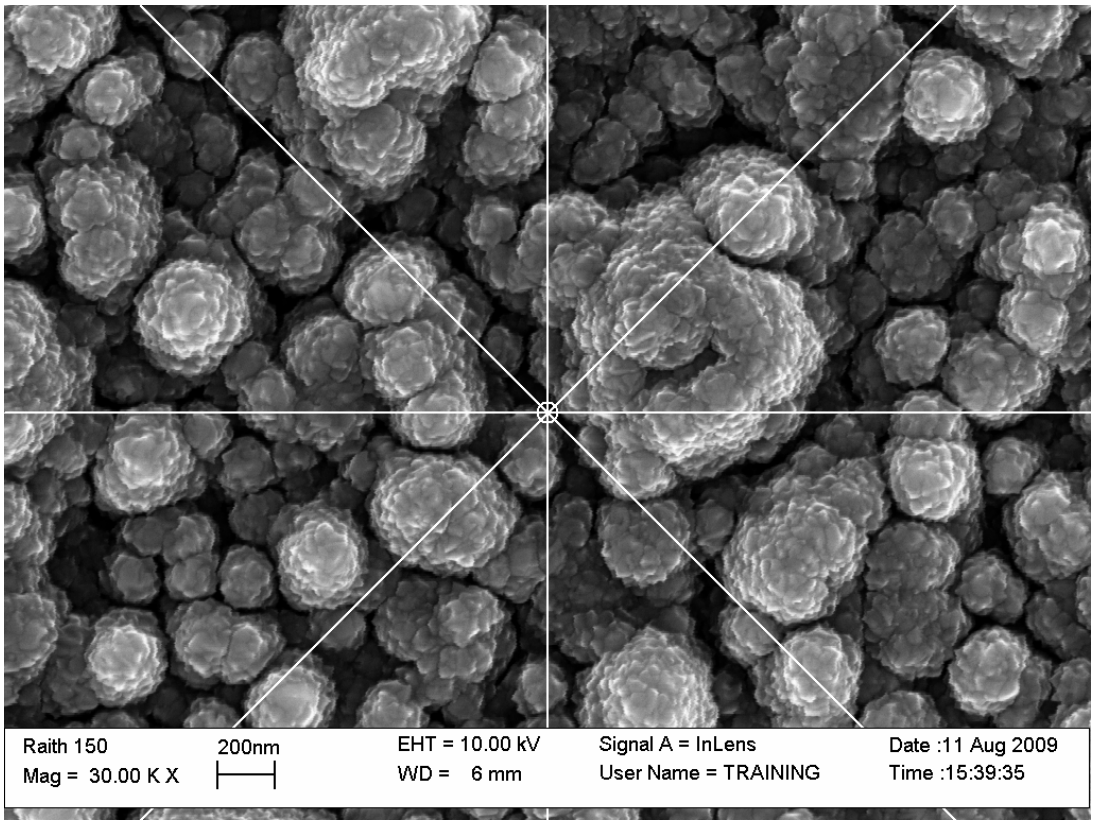

Figure 42 AZO 200 nm unannealed

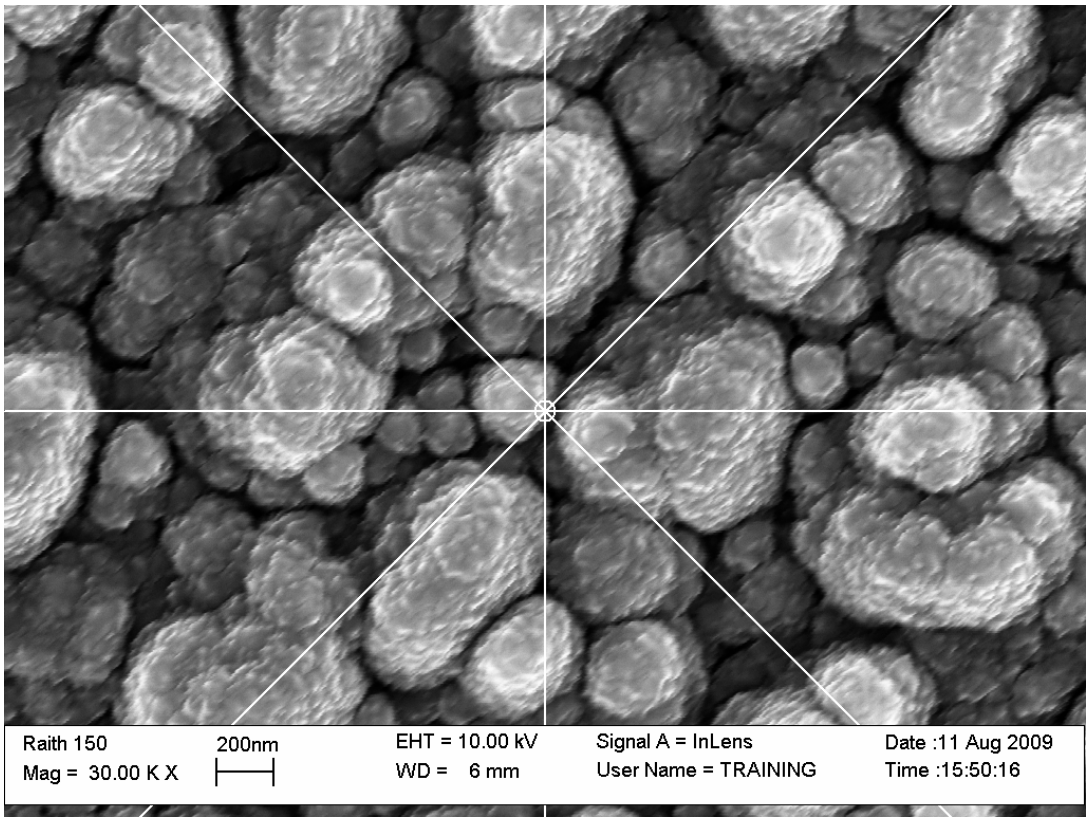

Figure 43 AZO 200nm annealed—no apparent difference at the first sight, but some small details of the Al:ZnO structure seem to disappeared

4.3 DSSC Cell Assembly

4.3.1 TiO_2 deposition on ITO glass

DSSC cells are first assembled with ITO glass as an example to be compared with the cells fabricated with textured substrates. Figure (44) shows the image of TiO_2 particles deposited on ITO glass.

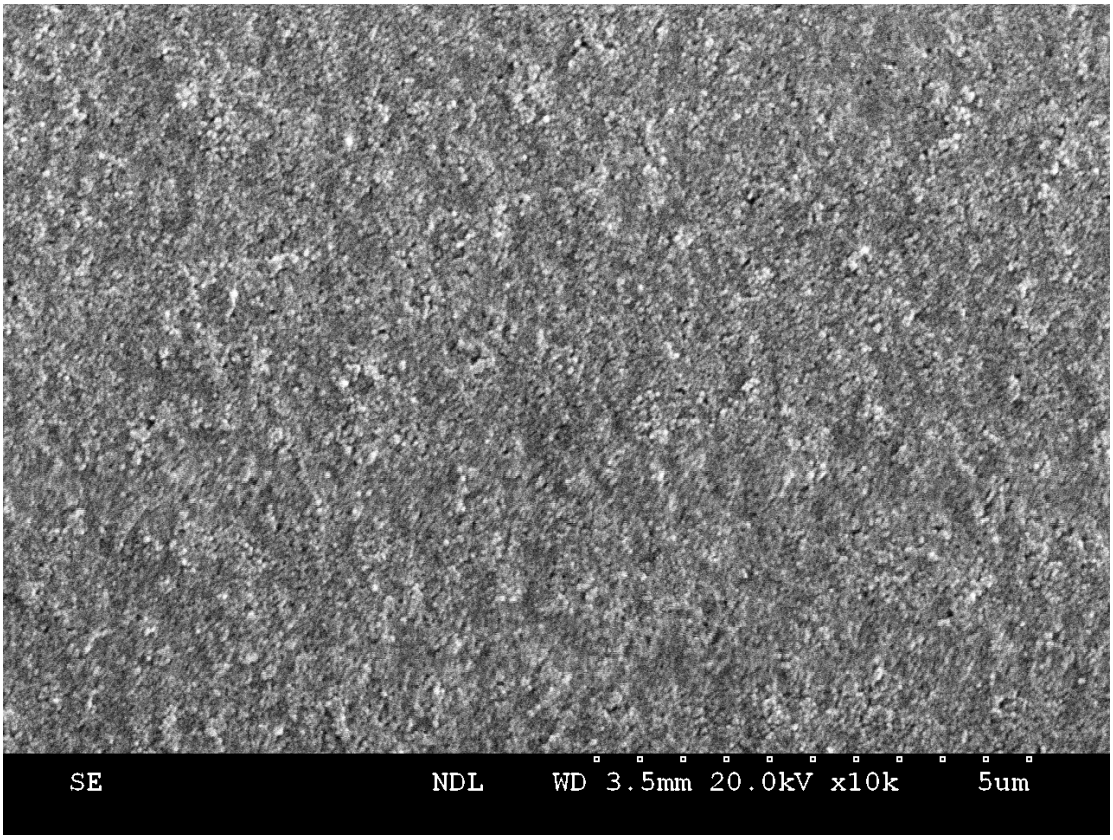

Figure 44 SEM image of TiO2 smoothly deposited on ITO glass—TiO_2 used in this research are mesoporous structure in nanoscale.

4.3.2 Difficulty on TiO_2 deposition

Different ways of stacking the cells were tried out. One of the biggest problems in DSSC assembly is that it is difficult to uniformly spin coat TiO_2 onto the Al:ZnO coated substrate surface, resulting in large particles on the surface, as shown in Figure (45). This creates difficulties in getting SEM image or AFM image as the film was

not uniformly spread out. There were not many literatures that dealt with such difficulty since the publications on Al:ZnO are mainly targeted at the film's optical and electrical properties. Adding extra amount of H_2O did not solve the problem as most of the solution is removed from the substrate by spinning. Increasing the spinning speed does help for coating one layer of uniform TiO_2 and sometimes could extended to 2 layers, but this is the maximum. Adding a third layer of TiO_2 would create cracks on the surface. However, due to the increase in speed, the thickness of each TiO_2 layer dramatically decreased to less than 1 μm resulting in thin semiconductor layer that is difficult to use in DSSC. Moreover, the increase in H_2O in the solution gives a rapid drop of the cell performance. In consequence, all the recordable cell performances (above 0.5% cell efficiency) are obtained from using etched substrates as the back reflector for the cell. Figure (46) shows the SEM image of TiO_2 on textured glass.

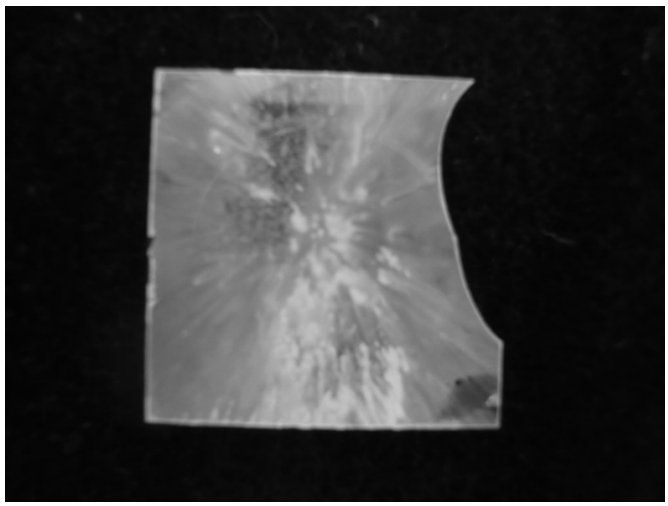

Figure 45 Photo image of TiO2 spin coated on AZO deposited substrate

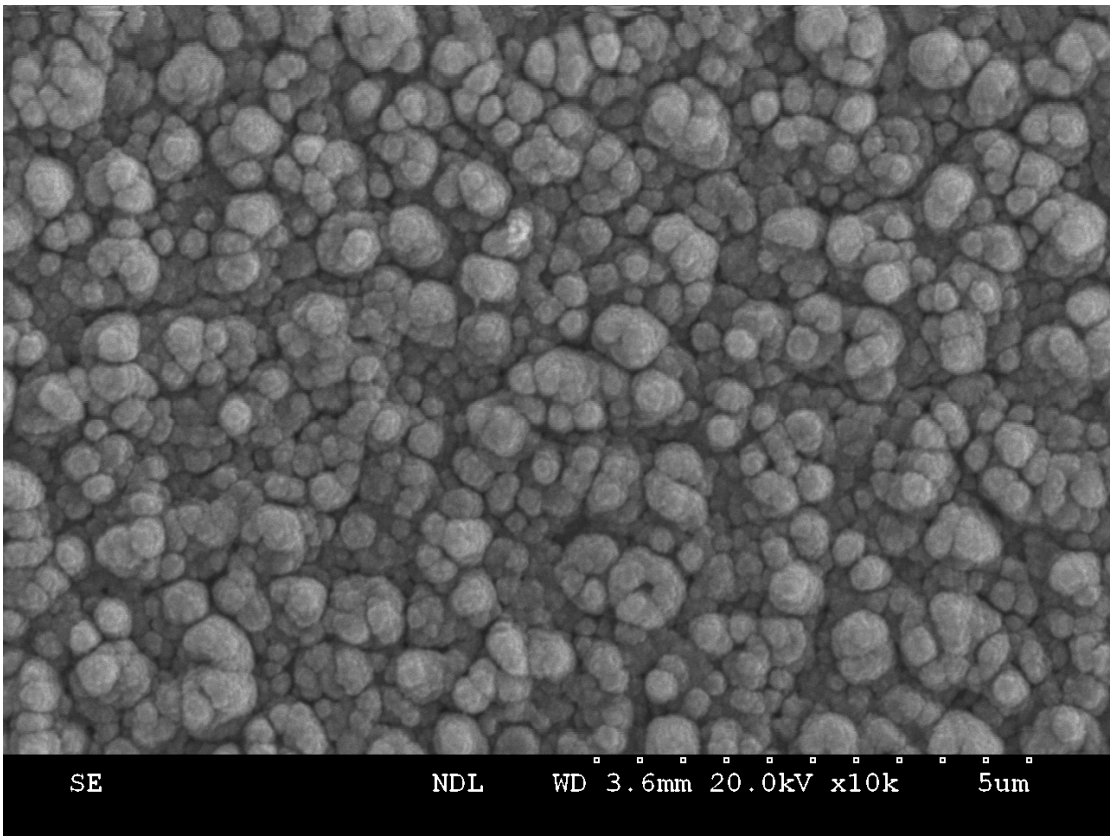

Figure 46 TiO2 deposited on RIE 1 hour textured glass, showing more detailed pattern in comparison with that on ITO glass

4.3.3 Cell Assembly: cell stacking and polymer heating

Due to the fact that the glass substrates used in this research are thin microscope cover glasses that are very fragile, usual cell assembly steps cannot be used for cell stacking. File clips were used to hold the top and bottom substrates together when the cell is fabricated with ITO glass and the dryer was used to melt the spacer that are placed between substrates. The clips cannot be used for holding the textured glass substrates together because the external forces provided by the clips are too strong for the fragile textured glass to handle. Moreover, the hot wind that flows from the dryer is sometimes too strong for the cell to handle and results in substrate cracking. The way of overcome such problem is using a 70 °C to 80 °C hotplate instead of the hair dryer. Hotplate was not used for ITO based cell fabrication because of the slow heat transfer of the ITO glass. Such problem can be omitted as textured glass is much thinner than the ITO glass. Since the hotplate has a flat surface, the sample can be pressed by hand. To make sure that the sample receives an uniform force across the whole sample, a large object with a flat surface can be used in between the

hand and the sample, as shown in Figure (47).

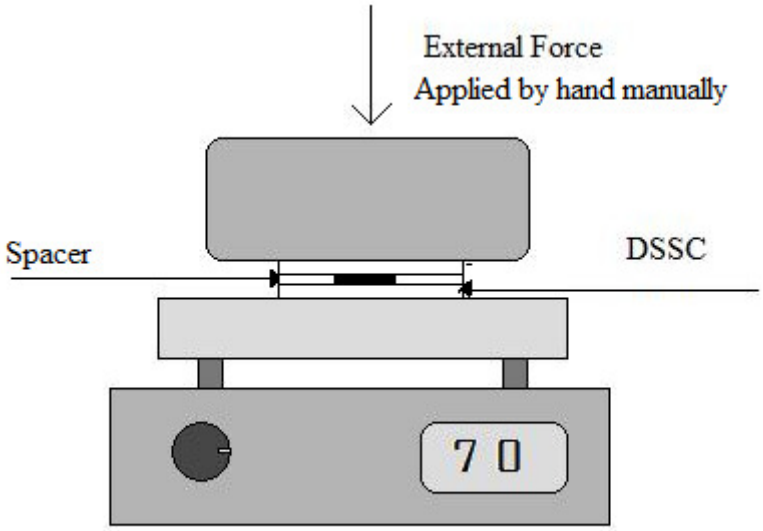

Figure 47 Placing the cell on the hotplate for few seconds with a flat surface object gently pressed from the top to melt the spacer and remove the air bubble

Spacers was left on the hot plate only for a few seconds due to the fact that it melts and expands during heating process and could block the channels specifically left for electrolyte injection, resulting in the inability of air bubble removal and liquid electrolyte injection. There was also a big concern on what should be used for applying external force on the cell while heating since uniform force is required for maximize the air bubble removal. After searching through various different objects, it was found that any objects such as wooden block, with a large flat surface can be used for distributing the applied force from hand evenly onto the sample.

4.3.4 Cell Performance

About half of the cells assembled could not be used in cell performance measurements due to various problems encountered during cell assembly such as TiO_2 coating and the way external force is applied to the cell (due to the fact that the microscope cover glass is very fragile). The most successful results are obtained when the substrates are used as the back substrates. The results are shown in Table (10). Front substrates are used for TiO_2 deposition and back substrates are for Pt sputtering. The effective area for the cell is 0.16 cm^2. There are many aspects that results in the low efficiency for no. 10 and no. 11, such as the TiO_2 coating problem

and the difficulty in cell assembly. Apart from the TiO_2 coating problem mentioned above, the resistivity of AZO is another big concern. Although the as deposited Al:ZnO resistivity is low, it rapidly increases to several kΩ after going through the 450 °C heat treatment after TiO_2 deposition.

	Front substrate	Back substrate	Voc (V)	Isc (mA)	Pmax (mW)	FF (%)	η (%)
1	ITO	ITO	0.6999	1.2260	0.8578	67.3337	3.6099
2	ITO	1hr surface textured glass with AZO 200	0.5999	0.0520	0.0078	24.7666	0.0485
3	ITO	1hr surface textured glass with AZO 400	0.7000	0.0007	0.2591	50.4774	1.6191
4	ITO	90 min surface textured glass with AZO 200	0.7499	0.0840	0.0154	24.4310	0.0959
5	ITO	90 min surface textured glass with AZO 400	0.7499	0.5810	0.4357	37.1426	1.0114
6	ITO	plain glass with AZO 200	0.6999	0.9730	0.2835	41.6279	1.7720
7	ITO	plain glass with AZO 400	0.6499	0.6030	0.1805	46.0211	1.1280
8	ITO	quartz with AZO 200	0.7000	1.0960	0.4151	54.1226	2.5941
9	ITO	quartz with AZO 400	0.7000	1.3670	0.4734	49.4795	2.9586
10	plain glass with AZO 200	ITO	0.8802	0.0005	0.0002	38.7120	0.0010
11	quartz with AZO 200	quartz with AZO 200	0.5499	0.0030	0.0004	25.4430	0.0024

Table 10 Performance results of DSSC fabricated

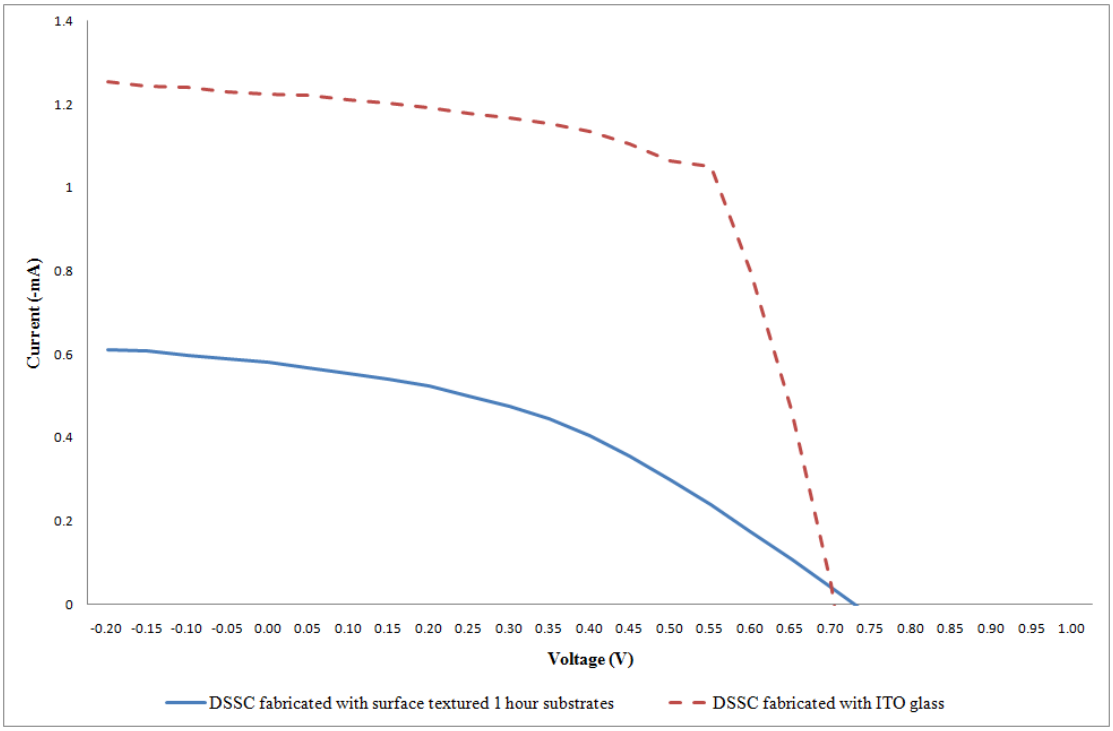

Figure 48 IV characteristics of DSSC fabricated with 1hr surface textured, 400 nm AZO coated glass in comparison with the performance of cell with ITO glass

DSSC fabricated with ITO as the top substrate and 1 hour surface textured glass coating with 400 nm of Al: ZnO as the bottom substrate is shown in Figure (48). The low short circuit current density may be due to the relatively high resistance of Al: ZnO.

In Figure (49), there is a clear difference in performance for cells fabricated with different back reflectors but coated with the same thickness of Al: ZnO. Plain quartz back reflector provides better results than cover glass. The cell fabricated with 90 minutes surface textured substrate did not give satisfactory result as shown in Figure (49) due to several problems during the cell assembly. Its low fill factor, 37.42%, indicates that the cell was not properly packaged as the ITO based cells. Apart from that the efficiency of the cell with 1 hour surface textured substrate seems to perform better than the cell composed of plain microscope cover glass, indicating an improvement in the performance of the cells.

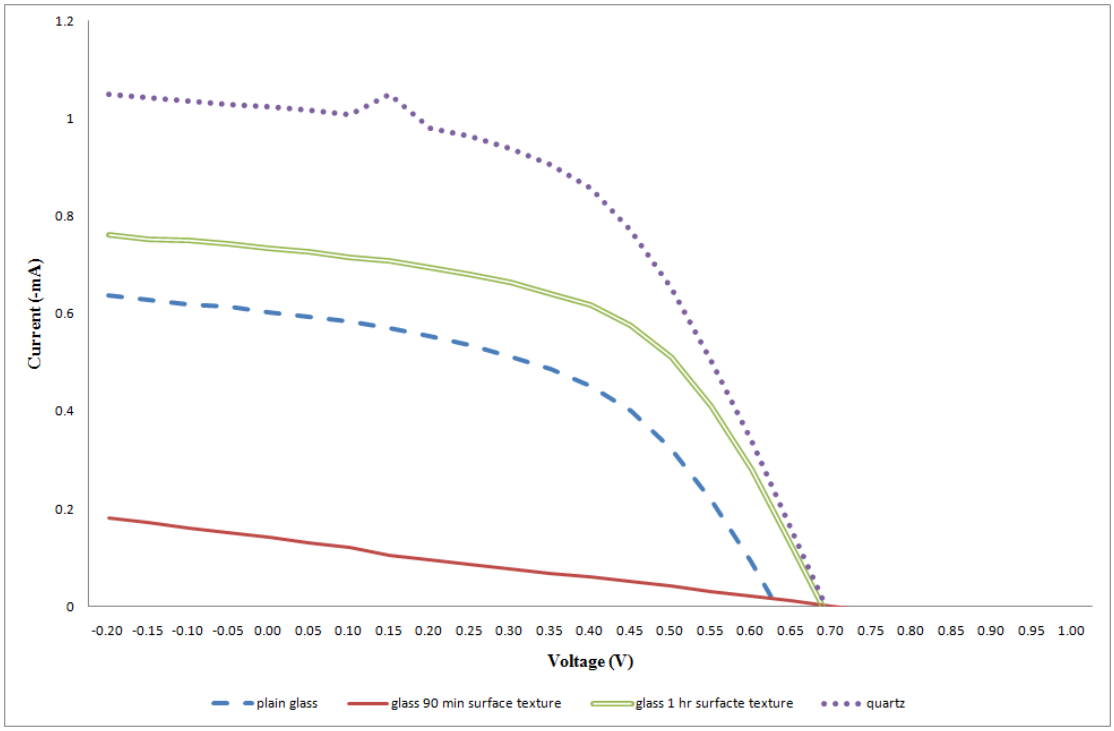

Figure 49 Efficiency of DSSC that are composed with different substrates coated with 400 nm Al: ZnO

There were not many satisfactory results for substrates coated with 200 nm Al: ZnO as most of the results are less than 0.1%. The results are compared in Figure (50) for performance of the cell composed of different substrates coated with 200 nm AZO. The straight lines of the cells with textured substrates indicates that the there is a huge

resistivity in the cells and that may due to the TCO resistivity and the improperly assembled cell. The fill factors of these cells are approximately 25%.

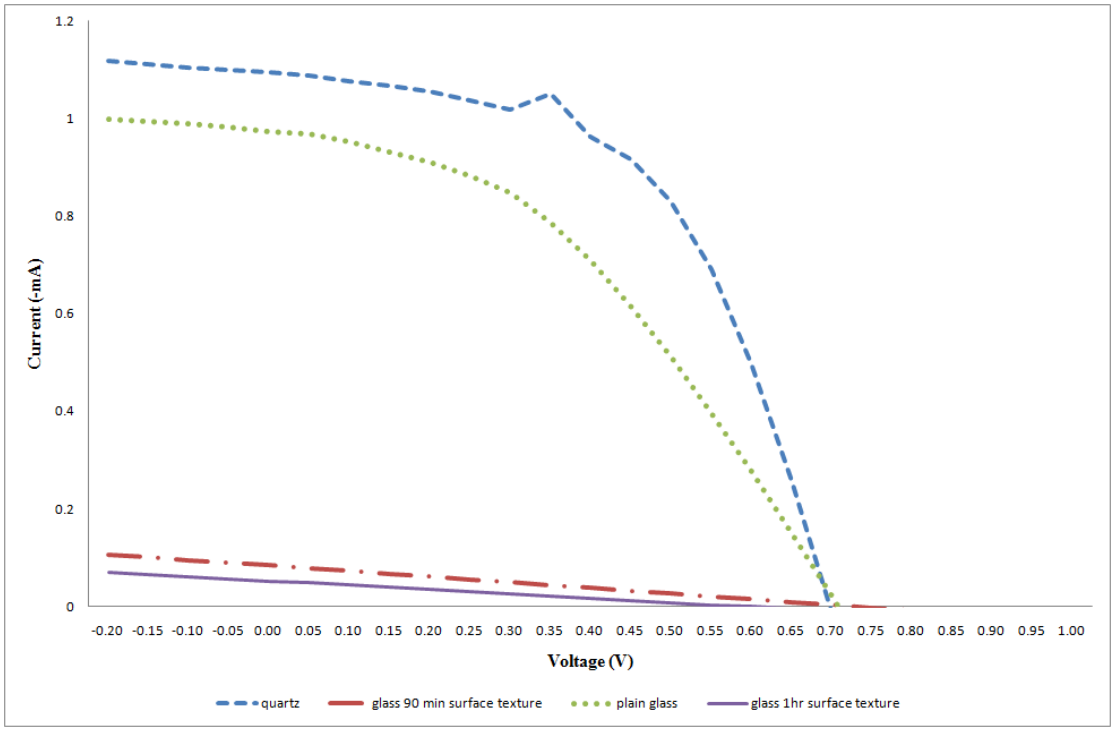

Figure 50 Different substrates coated with AZO 200 nm

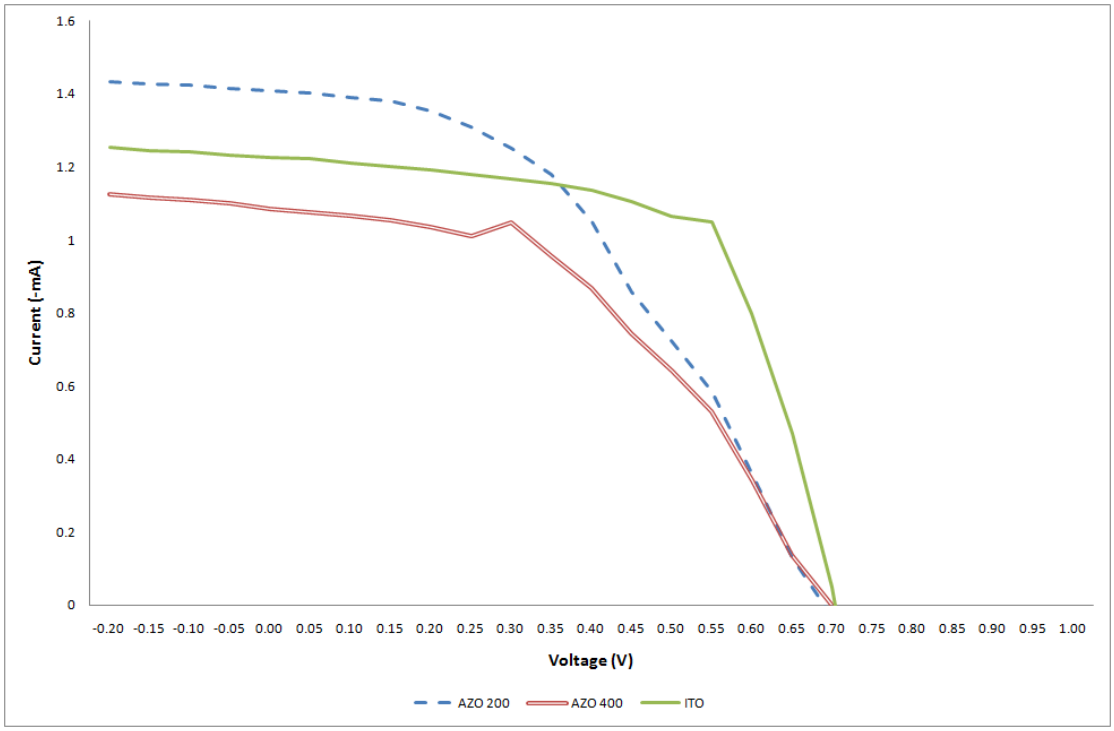

Figure 51 DSSC performance for cell fabricated with non textured microscope cover glass

The performance of cells with different Al: ZnO thickness on plane microscope glass is plotted in Figure (51). There was not much difference between the ITO based cell or Al: ZnO based cells but 200nm thick Al:ZnO gives more short circuit current density than other 400 nm thick AZO.

DSSCs are also fabricated on Al: ZnO coated quartz, as shown in Figure (52). It also shows a similar open circuit voltage as for the cells based on plain microscope cover glass. The efficiencies of the cells on quartz are generally better than those on microscope cover glass. This may be due to the fact that quartz substrates are slightly thicker and less fragile than the glass. Therefore, standard ITO based cell fabrication process can be used on quartz substrates.

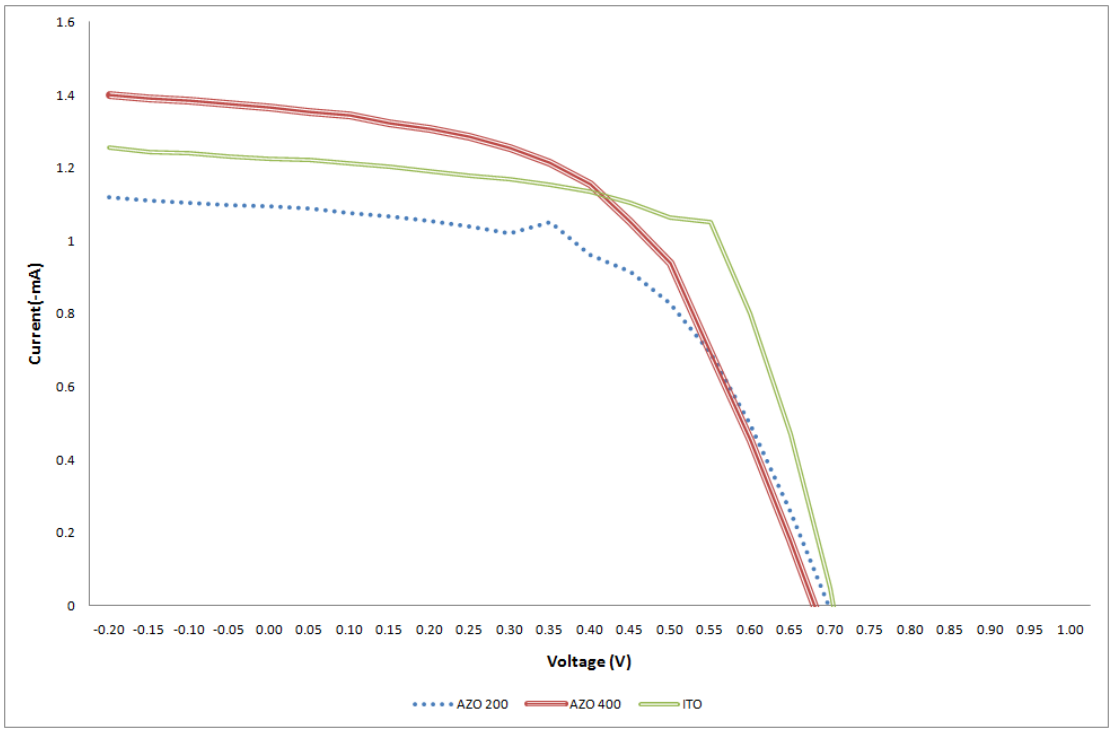

Figure 52 Comparison of cell efficiency between ITO glass and different thickness of AZO on quartz

There are very few results obtained from cells produced with Al: ZnO coated substrates as the top substrates due to the TiO_2 deposition problem. The best performances obtained from using Al:ZnO coated glass for TiO_2 deposition were all less than 0.01% efficiency like no. 10 and no. 11 in Table 10. Figure (53) and Figure (54) show the corresponding cell efficiencies of the samples. The straight line in Figure (54) indicates the existence of a huge resistance in the cell.

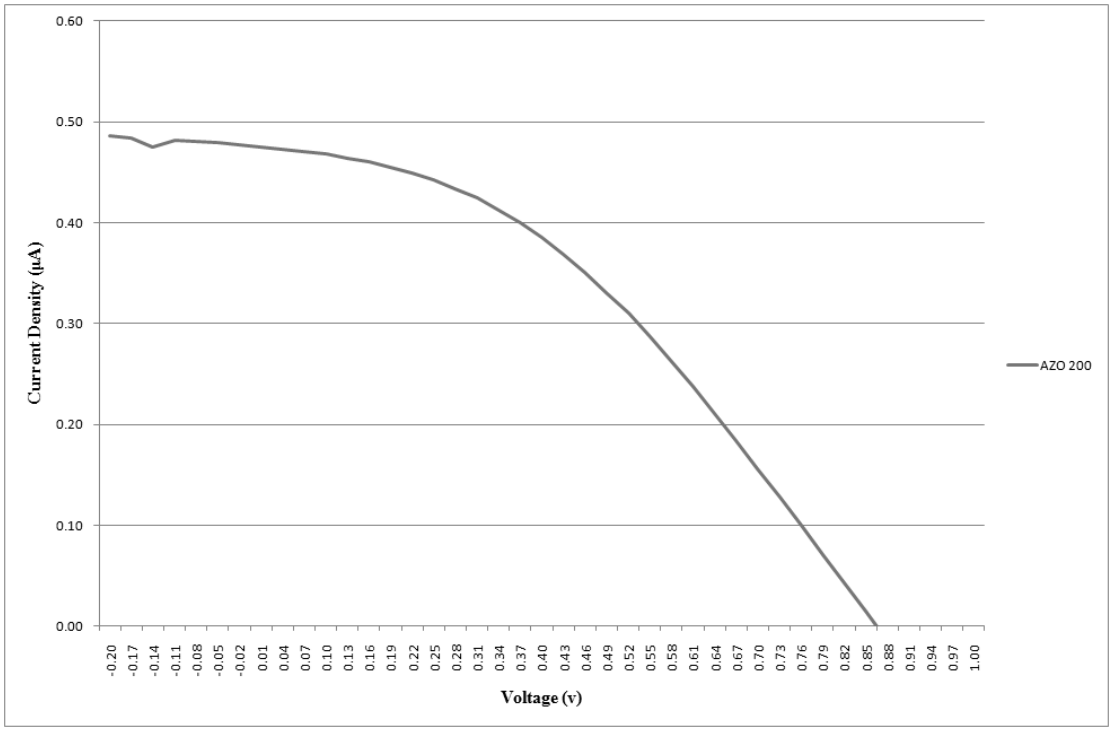

Figure 53 IV curve of the cell fabricated with 1 hour surface textured glass as the top substrate

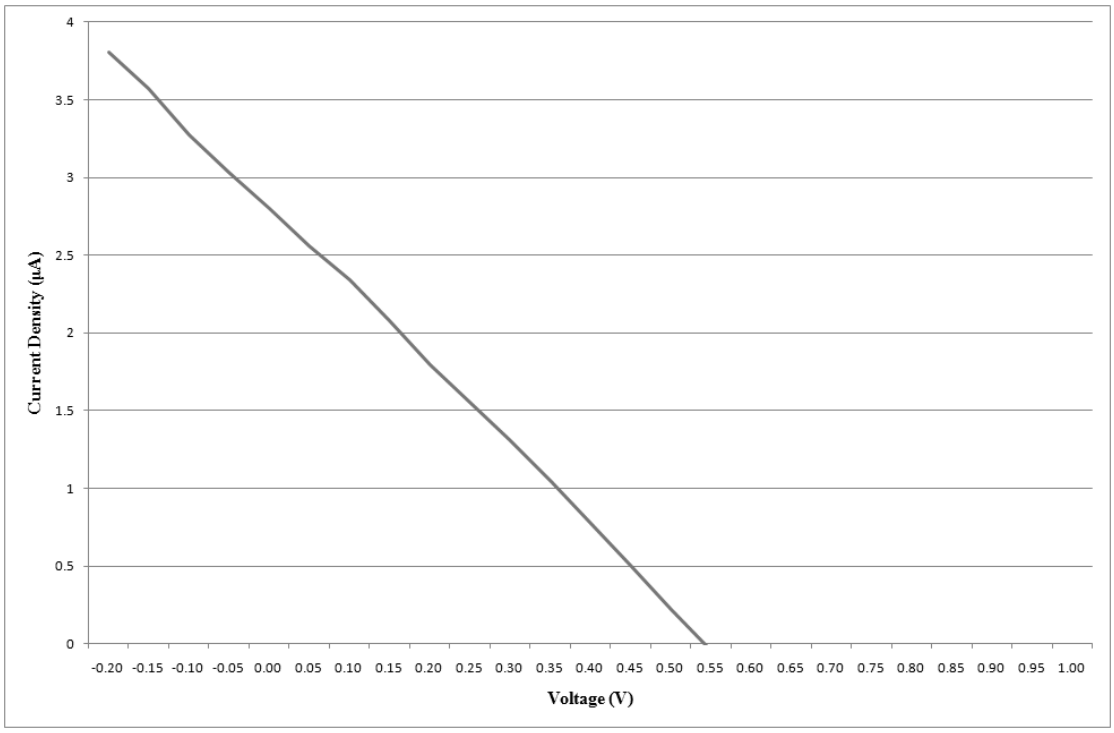

Figure 54 IV performance of DSSC fabricated with 1hour surface textured glass with 400 nm AZO coatings as top and bottom substrates

5. Conclusions and Future Works

5.1 Conclusions

Substrate surface texturing was successfully done by RIE without the presence of mask materials. The microscope cover glass was etched with RIE without using pre patterned mask and results obtained showed a decrease in reflectance. The Al:ZnO transparent conductive oxide was deposited at room temperature with RF magnetron sputtering. A decrease in reflectance, especially at near infrared region, was observed. Moreover, a different phase orientation of the material was observed on the Al:ZnO coated textured substrates. The SEM images of the substrate and Al:ZnO show interesting surface morphologies that were not found in the literatures, possibly due to the rough pattern on the substrates.

The fabrication process of DSSC was gradually adjusted so that the sample handling can be easier and the defects created during assembly can be minimized. The best performance of the samples was obtained from the cells assembled with ITO glass as top and bottom substrates. Most of the Al:ZnO coated substrates were used as back substrates instead of the top substrates as planned due to the difficulties in TiO_2 deposition. The efficiencies of these cells are approximately 1 % to 2 % lower than the original cell assembled with two ITO glass. Samples assembled with Al:ZnO coated glass as top and bottom substrates are difficult to obtain cell characteristics and the best efficiencies obtained from these samples are less than 0.01%.

Despite that there were several obstacles encountered with DSSC fabrication, the result still shows the possibility of improvement in DSSC and the outcome would be even more obvious with further adjustments.

5.2 Future Works

5.2.1 Optimizations

Since fabrication of DSSC using surface textured substrates is proved to be attainable, fine adjustments on current parameters can be done in the future for achieving optimal

results. This includes alternating the parameters, such as pressure, and the materials, such as substrate material (different glass compositions) and types of gas (SF_6 is another type of gas that is commonly used for glass etching), used for RIE etching. Different thickness of glass substrates can be used instead of the fragile microscope cover glass for easier fabrication handling purpose and for future commercialization. Different gas mixtures, such as SF_6/Ar, or CF_4/Ar, should be analyzed in comparison with the CHF_3/Ar mixtures to obtain optimal maskless RIE surface texturing in different substrates. The effect of pressure on surface texturing was not investigated in this research, so it would be good to see the effect of different pressure conditions in surface texturing.

The characteristics of Al:ZnO need to be improved for reducing the high resistance in DSSC. This includes electrical, optical and chemical properties. This may be done by trying out RF magnetron sputtering at different temperature and adjusting the annealing parameters to lower the resistivity and increase the transmittance. TiO_2 colloidal material can be replaced by commercialized paste instead of the solution and the coating method can be replaced by screen printing method instead of spin coating so that problem of inability to coat the material uniformly on Al:ZnO coated substrates can be ignored.

5.2.2 Applying Surface Texturing on Large Scale Substrates

Because the commercialized DSSC is fabricated either with large scale glass substrates or plastic rolls, and that the whole fabrication process is much different to the ones in laboratory, it would be interesting to see how the textured substrates improve the performance of large scale DSSC.

6. References

1. *Development of Solar Cells*. 2010; Available from: http://www.britannica.com/EBchecked/topic/552875/solar-cell.
2. *Bell Labs Top 10 Innovations*. 2010; Available from: http://www.alcatel-lucent.com/wps/portal/!ut/p/kcxml/04_Sj9SPykssy0xPLMnMz0vM0Y_QjzKLd4w3MXMBSYGYRq6m-pEoYgbxjggRX4_83FT9IH1v_QD9gtzQiHJHR0UAaOmbyQ!!/delta/base64xml/L3dJdyEvd0ZNQUFzQUMvNElVRS82X0FfNDZL.
3. *Painless Carbon Reduction by 80%*. 2010; Available from: http://www.internet-public-library.org/carbon-reduction/painless-carbon-reduction.htm.
4. Ohl, R., *Light Sensitive Electric Device*. 1946, 2402662: US patent.
5. Perlin, J., *The Silicon Solar Cell Turns 50*. 2004, National Renewable Energy Laboratory.
6. Yang, D., *Solar Cell Materials*. 2008: Wunan Book Co., Ltd.
7. Pankove, J.I. and D.E. Carlson, *Electroluminescence in amorphous silicon.* Applied Physics Letters, 1976. **29**(9): p. 620-622.
8. Muthmann, S. and A. Gordijn, *Amorphous silicon solar cells deposited with non-constant silane concentration.* Solar Energy Materials and Solar Cells. **In Press, Corrected Proof**.
9. Koch, C., M. Ito, and M. Schubert, *Low-temperature deposition of amorphous silicon solar cells.* Solar Energy Materials and Solar Cells, 2001. **68**(2): p. 227-236.
10. Dagamseh, A.M.K., et al., *Modelling and optimization of a-Si:H solar cells with ZnO:Al back reflector.* Solar Energy Materials and Solar Cells, 2010. **94**(12): p. 2119-2123.
11. Rockett, A.A., *Current status and opportunities in chalcopyrite solar cells.* Current Opinion in Solid State and Materials Science, 2010. **14**(6): p. 143-148.
12. Gu, H.T., *Introduction to Solar Cell Devices*. 2008: Chuan Way Book Co. Ltd.
13. Compaan, A.D., et al., *High efficiency, magnetron sputtered CdS/CdTe solar cells.* Solar Energy, 2004. **77**(6): p. 815-822.
14. Wu, X., *High-efficiency polycrystalline CdTe thin-film solar cells.* Solar Energy, 2004. **77**(6): p. 803-814.
15. Romeo, N., A. Bosio, and A. Romeo, *An innovative process suitable to produce high-efficiency CdTe/CdS thin-film modules.* Solar Energy Materials and Solar Cells, 2010. **94**(1): p. 2-7.

16. Flores Mendoza, M.A., et al., *Structural, morphological, optical and electrical properties of CdTe films deposited by CSS under an argon-oxygen mixture and vacuum.* Solar Energy Materials and Solar Cells. **In Press, Corrected Proof**.
17. Grätzel, M., *Dye-sensitized solar cells.* Journal of Photochemistry and Photobiology C: Photochemistry Reviews, 2003. **4**: p. 145 - 153.
18. O'Regan, B. and M. Grätzel, *A low-cost, high-efficiency solar cell based on dye-sensitized colloidal TiO2 films.* Nature, 1991. **353**(6346): p. 737-740.
19. Green, M. *The Future of Thin-film Solar Cells*. Solar Power 2006 2006; Available from: http://www.tvworldwide.com/events/eqtv/061016/.
20. König, D., et al., *Hot carrier solar cells: Principles, materials and design.* Physica E: Low-dimensional Systems and Nanostructures, 2010. **42**(10): p. 2862-2866.
21. Luque, A. and A. Martí, *Electron-phonon energy transfer in hot-carrier solar cells.* Solar Energy Materials and Solar Cells, 2010. **94**(2): p. 287-296.
22. Löffler, J., et al., *Amorphous and [`]micromorph' silicon tandem cells with high open-circuit voltage.* Solar Energy Materials and Solar Cells, 2005. **87**(1-4): p. 251-259.
23. Okamoto, S., et al., *Towards large-area, high-efficiency a-Si/a-SiGe tandem solar cells.* Solar Energy Materials and Solar Cells, 2001. **66**(1-4): p. 85-94.
24. Yanagida, M., et al., *Optimization of tandem-structured dye-sensitized solar cell.* Solar Energy Materials and Solar Cells, 2010. **94**(2): p. 297-302.
25. Florescu, M., et al., *Improving solar cell efficiency using photonic band-gap materials.* Solar Energy Materials and Solar Cells, 2007. **91**(17): p. 1599-1610.
26. Grätzel, M., *Photoelectrochemical cells*, in *NATURE*. 2001. p. 338-344.
27. Hagfeldt, A. and M. Grätzel, *Molecular Photovoltaics.* Accounts of Chemical Research, 2000. **33**(5): p. 269-277.
28. Hsiao, P.-T., et al., *Nanocrystalline anatase TiO2 derived from a titanate-directed route for dye-sensitized solar cells.* Journal of Photochemistry and Photobiology A: Chemistry, 2007. **188**(1): p. 19-24.
29. Wu, T., et al., *Photosensitization of TiO2 colloid by hypocrellin B in ethanol.* Journal of Photochemistry and Photobiology A: Chemistry, 2000. **137**(2-3): p. 191-196.
30. Mohammadi, M.R., et al., *Preparation of high surface area titania (TiO2) films and powders using particulate sol-gel route aided by polymeric fugitive agents.* Sensors and Actuators B: Chemical, 2006. **120**(1): p. 86-95.
31. Ahn, Y.U., et al., *Variation of structural and optical properties of sol-gel TiO2 thin films with catalyst concentration and calcination temperature.* Materials Letters, 2003. **57**(30): p. 4660-4666.

32. Nozawa, T. *DSC Research Accelerates; Better Efficiency, Durability*. 2009; Available from: http://techon.nikkeibp.co.jp/article/HONSHI/20090527/170862/.
33. *Dyesol Store*. Available from: https://secure.dyesol.com/.
34. Chen, Z.-t., *Molecular Co-sensitization of Mixed Organic Dyes for Dye-Sensitized Solar Cells*, in *Department of Chemical Engineering*. 2008, National Cheng Kung University: Tainan, Taiwan.
35. Ling, S.C., *The Assembly of Quantum dots and its Application in Dye Sensitized Solar Cell*, in *Chemical Engineering*. 2006, National Cheng Kung University: Tainan.
36. Suraprapapich, S., et al., *Quantum dot integration in heterostructure solar cells.* Solar Energy Materials and Solar Cells, 2006. **90**(18-19): p. 2968-2974.
37. Kingslake, R., *A history of the photographic lens*. 1989, Boston: Academic Press, Corp.
38. Abrahams, P. *H. Dennis Taylor, Optical Designer for T. Cooke & Sons*. Available from: http://home.europa.com/~telscope/hdtaylor.txt.
39. Kumaravelu, G., *Advanced Surface Texturing For Silicon Solar Cells*, in *Department of Electrical and Computer Engineering*. 2004, University of Canterbury: Christchurch. p. 156.
40. Thelen, A., *Design of Optical Interference Coatings*. 1989, Germany: McGRAW-HILL.
41. Dobrzański, L.A. and A. Drygała, *Surface texturing of multicrystalline silicon solar cells.* Journal of Achievements in Materials and Manufacturing Engineering, 2008. **31**(1): p. 77-82.
42. Green, M.A., *Silicon Solar Cells: Advanced Principles and Practice*. 1995, Sydney: Centre for Photovoltaic Device and Systems.
43. Badeker, K., *Concerning the electricity conductibility and the thermoelectric energy of several heavy metal bonds.* Annalen der Physik, 1907. **22**: p. 749.
44. Holland, L., *VACUUM DEPOSITION OF THIN FILMS*. 1st ed. 1963: Chapman & Hall Ltd. 555.
45. Sahu, D.R., S.-Y. Lin, and J.-L. Huang, *Investigation of conductive and transparent Al-doped ZnO/Ag/Al-doped ZnO multilayer coatings by electron beam evaporation.* Thin Solid Films, 2008. **516**(15): p. 4728-4732.
46. Sahu, D.R., S.-Y. Lin, and J.-L. Huang, *Study on the electrical and optical properties of Ag/Al-doped ZnO coatings deposited by electron beam evaporation.* Applied Surface Science, 2007. **253**(11): p. 4886-4890.
47. Subrahmanyam, A. and U.K. Barik, *Synthesis of P-type transparent conducting silver:indium oxide (AIO) thin films by reactive electron beam evaporation*

technique. Journal of Physics and Chemistry of Solids, 2005. **66**(5): p. 817-822.
48. May, C., et al., *Deposition of TCO films by reactive magnetron sputtering from metallic Zn:Al alloy targets.* Surface and Coatings Technology, 2003. **169-170**: p. 512-516.
49. Vaufrey, D., et al., *Reactive ion etching of sol-gel-processed SnO2 transparent conducting oxide as a new material for organic light emitting diodes.* Synthetic Metals, 2002. **127**(1-3): p. 207-211.
50. Dagkaldiran, Ü., et al., *Amorphous silicon solar cells made with SnO2:F TCO films deposited by atmospheric pressure CVD.* Materials Science and Engineering: B, 2009. **159-160**: p. 6-9.
51. Faÿ, S., et al., *Opto-electronic properties of rough LP-CVD ZnO:B for use as TCO in thin-film silicon solar cells.* Thin Solid Films, 2007. **515**(24): p. 8558-8561.
52. Agashe, C. and S. Mahamuni, *Competitive effects of film thickness and growth rate in spray pyrolytically deposited fluorine-doped tin dioxide films.* Thin Solid Films, 2010. **518**(17): p. 4868-4873.
53. Chen, S.C., *The properities of transparent ductivite oxides ITO deposited on flexible substrate*, in *Department of Materials Science and Engineering*. 2003, National Cheng Kung University: Tainan, Taiwan.
54. *Indium Tin Oxide Technology (ITO)*, in *BizEsp Limited*. 2007.
55. *Novel TCO film--FTO on glass*. Available from: http://www.materialsnet.com.tw/eng/FTO.html.
56. Tsai, F.Y., *The Study of Synthesis of Fluorine-doped Tin Oxide Nanowires and the Electrical Property of a Single Fluorine-doped Tin Oxide Nanowire*, in *Department of Engineering and System Science*. 2008, National Ching Hua University: Hsinchu, Taiwan.
57. Lin, S.S., *The Investigation for Improving Properties and Application of Zinc Oxide Films*, in *Materials Science and Engineering*. 2003, National Cheng Kung University: Tainan, Taiwan.
58. Suchea, M., et al., *Comparative study of zinc oxide and aluminum doped zinc oxide transparent thin films grown by direct current magnetron sputtering.* Thin Solid Films, 2007. **515**(16): p. 6562-6566.
59. Ryan, M., *PGM HIGHLIGHTS: Progress in Ruthenium Complexes for Dye Sensitised Solar Cells.* Platinum Metals Review, 2009. **53**(4): p. 216-218.
60. Tsai, S.Y., *Research on DSSC*. 2008, Industrial Technology Research Institute.
61. Wu, J., et al., *Progress on the electrolytes for dye-sensitized solar cells.* Pure and Applied Chemistry, 2008. **80**(11): p. 2241-2258.
62. Haug, F.-J., et al. *Stability of transparent front contacts for Cu(In,Ga)Se2 superstrate solar cells* in *Proceedings of the 16th European Photovoltaic Solar*

Energy Conference. 2000. Glasgow.

63. Ozgur, U., et al., *A comprehensive review of ZnO materials and devices.* Journal of Applied Physics, 2005. **98**(4): p. 103.
64. *RIE Reactive Ion Etcher*. Available from: http://www.oxfordplasma.de/technols/rie.htm.
65. *MEMs Technology: Chapter 4 Etching Technology*. 2002; Available from: http://elearning.stut.edu.tw/m_facture/Nanotech/Web/ch4.htm.
66. Lo, J.-T., *Thin Film Technology and Application*. 2009: Chuanwa Book CO. Ltd.
67. Faculty of Physics, R.A.U., *The reactive DC-Magnetron Sputtering Process*.
68. Center for Engineering and Physical Science Research, C.U., *Spin Coat Theory*.
69. Blanchard, C.R., *Atomic Force Microscopy.* The Chemical Educator, 1996. **1**(5): p. 1-8.
70. Breton, B. *The Early History and Development of The Scanning Electron Microscope*. 2009.
71. Leung, B. *Field Emission Scanning Microscopy/Energy Dispersive X-ray Analysis (FESEM/EDX)*. 2010; Available from: http://www.hkbu.edu.hk/~csar/fesem.html.
72. *HALL EFFECT MEASUREMENTS*, in *Lake Shore 7500/9500 Series Hall System User's Manual*. p. A1-A18.
73. Thurber, W.R. *Hall Effect Measurements Resistivity*. Available from: http://www.nist.gov/pml/semiconductor/hall.cfm.
74. Wu, Y.D., *Preparation of CuInS2 absorber using successive ionic layer adsorption and reaction method for application in extremely thin absorber solar cells*, in *Department of Chemical Engineering*. 2007, National Cheng Kung University: Tainan, Taiwan.
75. *Uni-Onward Corp.*; Available from: www.uni-onward.com.tw.
76. Hsieh, C.G., *Optical and Electrical Characteristics Analysis of Al:ZnO Transparent Conductance Oxide Film*, in *Department of Photonics* 2005, National Chung Yang University.
77. Lin, S.S., *The Investigation for Improving Properties and Applications of Zinc Oxide Films*, in *Department of Materials Science and Engineering*. 2003, National Cheng-Kung University: Tainan.
78. *V-670 SPECTROPHOTOMETER*. Available from: http://www.jascoinc.com/Products/Spectroscopy/V-600-Spectrophotometer-Series.aspx.
79. *Information Materials*. Available from: http://ccsun.nchu.edu.tw/~imtech/.
80. *Fully Reflective Solar Simulator 150W* Available from: http://www.sciencetech-inc.com/en/catalog/1/solar_simulators/SS150.

81. *Solar Simulator Manufacturer: Fully Reflective Technology*, S. Inc., Editor, ScienceTech Inc.
82. Gatzert, C., et al., *Investigation of reactive ion etching of dielectrics and Si in CHF3/O2 or CHF3 /Ar for photovoltaic applications.* J. Vac. Sci. Technol. A, 2006. **24**(5): p. 1857-1865.
83. Ronggui, S. and G.C. Righini, *Characterization of reactive ion etching of glass and its applications in integrated optics.* J. Vac. Sci. Technol. A, 1991. **9**(5): p. 2709-2712.
84. Singh, A.V., et al., *Al-doped zinc oxide (ZnO:Al) thin films by pulsed laser ablation.* J. Indian Inst. Sci., 2001. **81**: p. 527-533.
85. Czternastek, H., *ZnO thin films prepared by high pressure magnetron sputtering.* 2004. **12**(1): p. 49-52.
86. Mondal, S., K.P. Kanta, and P. Mitra, *Preparation of Al-doped ZnO (AZO) Thin Film by SILAR.* Journal of Physical Sciences, 2008. **12**: p. 221-229.